Department of Applied Physics

Modelling of JET and ITER reactor relevant plasma neutron source for neutronics calculation chain

Paula Sirén

Aalto University

DOCTORAL DISSERTATIONS

Aalto University publication series
DOCTORAL DISSERTATIONS 118/2018
VTT SCIENCE 180

Modelling of JET and ITER reactor relevant plasma neutron source for neutronics calculation chain

Paula Sirén

A doctoral dissertation completed for the degree of Doctor of Science (Technology) to be defended, with the permission of the Aalto University School of Science, at a public examination held at the lecture hall M1 of the school on 19 June 2018 at 13.

Aalto University
School of Science
Department of Applied Physics
VTT Reactor Physics

Supervising professor
Prof. Filip Tuomisto, Aalto University, Finland

Thesis advisor
Dr. Jaakko Leppänen, VTT Technical Research Centre of Finland Ltd, Finland

Preliminary examiners
Dr. Sean Conroy, Uppsala University, Sweden
Dr. Elina Militello-Asp, CCFE, UK

Opponent
Dr. Massimo Nocente, University Milano Bicocca, Italy

Aalto University publication series
DOCTORAL DISSERTATIONS 118/2018

VTT SCIENCE 180

ISBN 978-952-60-8046-8 (printed)
ISBN 978-952-60-8047-5 (pdf)
ISSN 1799-4934 (printed)
ISSN 1799-4942 (pdf)
http://urn.fi/URN:ISBN:978-952-60-8047-5

ISBN 978-951-38-8651-6 (printed)
ISBN 978-951-38-8650-9 (pdf)
ISSN 2242-119X (printed)
ISSN 2242-1203 (pdf)
http://urn.fi/URN:ISBN:978-951-38-8650-9

Images: Paula Sirén

Unigrafia Oy
Helsinki 2018

Finland

441 697
Printed matter

Aalto University

Abstract

Aalto University, P.O. Box 11000, FI-00076 Aalto www.aalto.fi

Author
Paula Sirén

Name of the doctoral dissertation
Modelling of JET and ITER reactor relevant plasma neutron source for neutronics calculation chain

Publisher School of Science

Unit Department of Applied Physics

Series Aalto University publication series DOCTORAL DISSERTATIONS 118/2018

Field of research Fusion and Plasma Physics

Manuscript submitted 18 April 2017 **Date of the defence** 19 June 2018

Permission to publish granted (date) 11 January 2018 **Language** English

☐ **Monograph** ☒ **Article dissertation** ☐ **Essay dissertation**

Abstract

It is essential for the research of reactor relevant plasmas to understand how heat transfer is affected by the properties of and phenomena in the plasma fuel. The major part of heat is transferred out via energetic neutrons. The neutrons must be taken into account as a heat source as well as from the perspective of material activation and induced reactions. In simulations the calculation chain from the reactants to products, heat transfer and material effects requires the coupling methods in plasma physics, reactor analysis and thermohydraulics calculation.

This thesis focuses on reactor relevant plasmas. The first part discusses plasma operational scenarios concentrating especially on advanced tokamak scenarios. The time evolution of the safety factor q is strongly connected to total plasma current and confinement, so the data analysis based on the identity plasma experiments is extended with predictive current diffusion simulations. A sensitivity test with respect to typical plasma parameters carried out for time evolution of q and internally generated bootstrap current density.

The second and third parts consider fusion products and their characterisation. The simulation tool AFSI fusion source integrator is presented and validated using JET tokamak data. The production rate and neutron spectrum is calculated in a geometry which correspond to real diagnostics based on the experimental data. Additionally, the results have been compared qualitatively to the experimental measurements when with good agreement between calculated and measured values.

In the fourth part, the calculation chain from the modelling of plasma fuel to the balance-of-plant modelling is described with the focus on the coupling of plasma physics and neutronics. As a demonstration case, the predictions ITER plasma data and a CAD model have been used. AFSI has been coupled to the ASCOT particle following code, which defines the distribution and energy of the reactants. A neutron source was provided for a dose-rate calculation with the Serpent code, which is available for a further coupling to thermohydraulics.

Keywords Plasma physics, magnetic confinement, scenario modelling, fusion neutrons, synthetic diagnostics

ISBN (printed) 978-952-60-8046-8 **ISBN (pdf)** 978-952-60-8047-5

ISSN (printed) 1799-4934 **ISSN (pdf)** 1799-4942

Location of publisher Helsinki **Location of printing** Helsinki **Year** 2018

Pages 126 **urn** http://urn.fi/URN:ISBN:978-952-60-8047-5

Tekijä
Paula Sirén

Väitöskirjan nimi
Modelling of JET and ITER reactor relevant plasma neutron source for neutronics calculation chain

Julkaisija Perustieteiden korkeakoulu

Yksikkö Teknillinen fysiikka

Sarja Aalto University publication series DOCTORAL DISSERTATIONS 118/2018

Tutkimusala Fuusio- ja plasmafysiikka

Käsikirjoituksen pvm 18.04.2017 **Väitöspäivä** 19.06.2018

Julkaisuluvan myöntämispäivä 11.01.2018 **Kieli** Englanti

☐ **Monografia** ☒ **Artikkeliväitöskirja** ☐ **Esseeväitöskirja**

Tiivistelmä

Reaktorikelpoisten fuusioplasmojen tutkimuksessa on olennaista ymmärtää plasmapolttoaineen ominaisuuksien ja ilmiöiden yhteys lämmönsiirtoon. Suurin osa lämmöstä kulkeutuu plasmasta fuusioreaktiossa tuotettujen suurienergisten neutronien mukana. Neutronit täytyy huomioida useammasta eri näkökulmasta: lämpölähteenä, materiaalien aktivoijana ja reaktioiden aiheuttajana. Laskentaketju plasman reagoivien ionien mallinnuksesta reaktiotuotteisiin, lämmönsiirtoon ja materiaalivaikutuksiin vaatii plasmafysiikan, reaktorianalyysin ja termohydrauliikan laskentamenetelmien yhdistämistä.

Tämä opinnäyte keskittyy reaktorikelpoisten plasmojen tarkasteluun. Ensimmäinen osa käsittelee plasmaskenaarioita, joista pääpaino on kehittyneillä tokamak-skenaarioilla. Varmuustekijän q aikakehityksellä on voimakas yhteys kokonaisplasmavirtaan ja plasman koossapitoon, joten plasmojen identiteettikokeisiin pohjautuvaa data-analyysia on laajennettu prediktiivisillä virtadiffuusiosimulaatioilla. Simulaatioilla on tehty herkkyystestejä parametrien vaikutuksesta varmuustekijän q aikakehitykseen ja sisäsyntyisen bootstrap-virran suuruuteen.

Toinen ja kolmas osa esittelevät fuusiotuotteet ja niiden karakterisointiin käytettävät menetelmät. Aluksi esitellään AFSI-fuusiotuotekoodi, joka on validoitu JET-tokamakilla. Koodia on sovellettu synteettiseen neutronidiagnostiikkaan JET-tokamakilla. Neutroneiden, tuottonopeus ja spektri on laskettu todellisia diagnostiikkainstrumentteja vastaavissa geometrioissa käyttäen plasmakokeiden dataa. Lisäksi laskentatuloksia on verrattu kvalitatiivisesti kokeellisesti arvoihin ja todettu menetelmien vastaavan hyvin mitattuja arvoja eri detektoreja vastaavissa sijainneissa.

Neljännessä osassa kuvataan kokonaisuudessaan laskentaketju plasmaparametrien mallinnuksesta laitoksen termohydrauliikkaan painottuen erityisesti plasmafysiikan ja neutronien kulkeutumisen mallinnuksen kytkemiseen. Esimerkkitapauksena on käytetty ITER-tokamakin ennustettuja plasmaparametreja ja rakennemallia. AFSI on kytketty ASCOT-hiukkasseurantakoodiin, joka määrittää reagoivien hiukkasten sijainnin, tiheyden ja energiat. Fuusiotuotteiden perusteella on muodostettu neutronilähde Serpent-neutronitransportkoodille, jota on käytetty reaktorinkomponenttien annosnopeuslaskun suorittamiseen, joka voidaan kytkeä edelleen termohydrauliikkamalliin.

Avainsanat Plasmafysiikka, magneettinen koossapito, fuusioneutronit, skenaariomallinnus, synteettiset diagnostiikat

ISBN (painettu) 978-952-60-8046-8 **ISBN (pdf)** 978-952-60-8047-5

ISSN (painettu) 1799-4934 **ISSN (pdf)** 1799-4942

Julkaisupaikka Helsinki **Painopaikka** Helsinki **Vuosi** 2018

Sivumäärä 126 **urn** http://urn.fi/URN:ISBN:978-952-60-8047-5

Acknowledgements

This work has been carried out within the framework of the EUROfusion Consortium and has received funding from the Euratom research and training programme 2014 -2018 under grant agreement number 633053 and from Tekes – the Finnish Funding Agency for Innovation under the FinnFusion Consortium . The views and opinions expressed herein do not necessarily reflect those of the European Commission. T he calculations presented here were performed in part using computer resources within the Aalto University School of Science "Science-IT" project.

Completing this thesis has been quite a long process and I would like to thank all the people who have contributed to the research related my work. Generally, I am grateful for all my colleagues at VTT, the Aalto ASCOT group and JET for their help.

I want to thank Dr Petri Kotiluoto (VTT), the leader of the reactor physics team, to provide the possibility to work on these studies under his group at VTT. I am also grateful for my advisors Dr Jaakko Leppänen (VTT) for his role as an advisor of the thesis and introducing me to neutronics, and Markus Airila (VTT) for his help especially with various practical problems related to PhD studies with my diverse topic. I would like to thank Dr Tuomas Tala (VTT) and Dr Xavier Litaudon (EUROfusion PMU) for their help and instruction to the topic related to the first part of thesis, and special thanks to my unofficial supervisor at JET, Henri Weisen (EPFL), for his help and support with a major part of this thesis during my long period at JET in 2016. Finally, I would like to say thank you to my pre-examinators Dr Elina Militello-Asp (CCFE) and Dr Sean Conroy (Uppsala University) and my opponent Dr Massimo Nocente (University Milano Bicocca) who were able to make the thesis much better with their important and valuable comments.

Oxford, 24 May 2018
Paula Sirén

Contents

List of Abbreviations and Symbols

a	minor radius
α	alpha particle
$B, \vec{B}_{tot}$	total magnetic field
B_φ	toroidal magnetic field
B_θ	poloidal magnetic field
β	beta factor, fraction of magnetic and kinetic pressure
β_N	normalised beta factor
β_θ	beta factor with the poloidal magnetic pressure
D	deuterium
D	particle diffusion coefficient
$E, \vec{E}$	electric field
E_φ	toroidal electric field
e	elementary charge
F	current flux function
f	distribution function
f_L	Larmor frequency
H_{98}	H factor, confinement scaling
I_{tot}, I	total plasma current
I_{bs}	bootstrap current
I_{ext}	externally produced current
I_{ohm}	inductive current
$\vec{J}$	current density vector
j_{bs}	bootstrap current density

$j_{bs,approx}$	approximation of bootstrap current density
j_{ext}	externally produced current density
j_{ohm}	inductive current density
M	mutual induction coefficient
m_j	mass of particle j
μ_0	vacuum permeability
n	neutron
n_{tot}	density
n_e	electron density
n_i	ion density
n_{tr}	trapped particle density
η	neoclassical resistivity
p	pressure
$\vec{p}$	momentum
ρ	toroidal normalised magnetic flux
ρ_*	normalised Larmor radius
ρ_L	Larmor radius
ϕ	toroidal magnetic flux
ψ	poloidal magnetic flux
Q	fusion gain
q	safety factor
q_{95}	safety factor at the toroidal flux $\rho = 0.95$
q_j	charge of particle j
R	major radius
R_0	major radius coordinate
R_{Th}	production rate in thermal particle reactions
$R_{Th-fast}$	production rate in thermal-fast particle reactions
R_{fast}	production rate in fast particle reactions
r	minor radius coordinate
s	magnetic shear

σ	cross section
$\langle \sigma v \rangle$	velocity averaged cross section
t	time
T_e	electron temperature
T_i	ion temperature
τ_E	energy confinement time
V	plasma volume
v_{CM}	velocity in center of mass coordinate system
$\vec{v}$	velocity vector
$v_{\parallel}$	parallel velocity with respect to the magnetic field
$v_{\perp}$	perpendicular velocity with respect to the magnetic field
ν	collisionality
ν_*	normalised collisionality
ν_{ei}	electron-ion collision frequency
χ	heat transport coefficient

List of Publications

This doctoral dissertation consists of a summary and of the following publications which are referred to in the text by their numerals

1. P. Sirén, T. Tala, G. Corrigan, J. Garcia,T. Koskela, F. Köchl, X. Litaudon, A. Salmi, JET EFDA contributors and the EU-ITM ITER Scenario Modelling Group. 2015. Understanding of the fundamental differences in JET and JT-60U AT discharges. Plasma Physics and Controlled Fusion 57 075015.

2. P. Sirén, J. Varje, S. Äkäslompolo, O. Asunta, C. Giroud, T. Kurki-Suonio, H. Weisen. 2018. ASCOT Fusion source integrator AFSI for fast ion and neutron studies in fusion devices. Nuclear Fusion 58 016023.

3. P. Sirén, J. Varje, H. Weisen, T. Koskela. 2017. Synthetic neutron camera and spectrometer in JET based on AFSI-ASCOT simulations. Journal of Instrumentations 12 C09010.

4. P. Sirén, J. Leppänen. Expanding the use of Serpent 2 to fusion applications: Development of a neutron source. In proc. PHYSOR 2016, Sun Valley, ID, May 1-6, 2016.

Author's Contribution

Publication 1: Understanding of the fundamental differences in JET and JT-60U AT discharges

The Author has done the analysis and simulations based on the experimental results and discussion with co-authors. The Author also wrote the manuscript as a main author.

Publication 2: ASCOT Fusion source integrator AFSI for fast ion and neutron studies in fusion devices

The Author was responsible for mathematical methods, validation and applications (including the manuscript without chapters 2.1 and the beginning of 3.2). The Author was a responsible author of the publication.

Publication 3: Synthetic neutron camera and spectrometer in JET based on AFSI-ASCOT simulations

The Author implemented and tested synthetic diagnostics and the Author was a responsible author and wrote the manuscript.

Publication 4: Expanding the use of Serpent 2 to fusion applications: Development of a neutron source

The Author is responsible for the neutron source part: implementing a source routine and simulations for defining probabilities for the demonstration cases. The Author was responsible for manuscript.

1. Introduction

1.1 Challenges in energy production now and in the future

Energy consumption has increased by almost 500% during the last 150 years in the largest countries in Europe. Correspondingly, CO_2 emissions have increased globally over 150 times from 1850 to 2011. Nowadays, energy consumption is increasing most rapidly in developing countries. For example, in 1850's in the beginning of industrialisation, England was the largest CO_2 emitter, whereas in 2000's, more than half of the emissions are coming from developing countries in Asia, where similar facilities or financial resources do not exist for controlling CO_2 and small particle air pollution. [1-2]

Together with CO_2 emissions, outdoor air pollution, especially small particle emissions, leads to serious problems with global warming and increased amount of premature deaths. For example, in the selected regions in China, the amount of premature deaths due to outdoor pollutions would be expected to increase by even close to 40% until 2040. Hence, there is a strong demand for carbon free and environmental friendly energy production methods for both growing industry and civilisation. [2-4]

In the 1900's, the major part of energy was produced by fossil fuels. Even in 2000's, up to 70% of investments in new energy supply projects has been spent in fossil fuels [3]. Due to global warming and particle emissions, this is an untenable solution. Renewable fuels, such as solar, water and wind power, cannot provide regular base-load power for energy intensive industry but they are also strongly dependent of location and general conditions. Nuclear fission power does not have particle or CO_2 emissions but the used radioactive fuel requires special long-term consideration and additionally it has a politically insecure reputation due to some serious accidents. Nuclear fusion is a promising solution: the fuel (hydrogen) is cheap and easy to purchase and the energy content per amount of fuel is remarkably large. Nevertheless, it has many technical challenges to solve before the first fusion energy power plants can be taken into use for energy production.

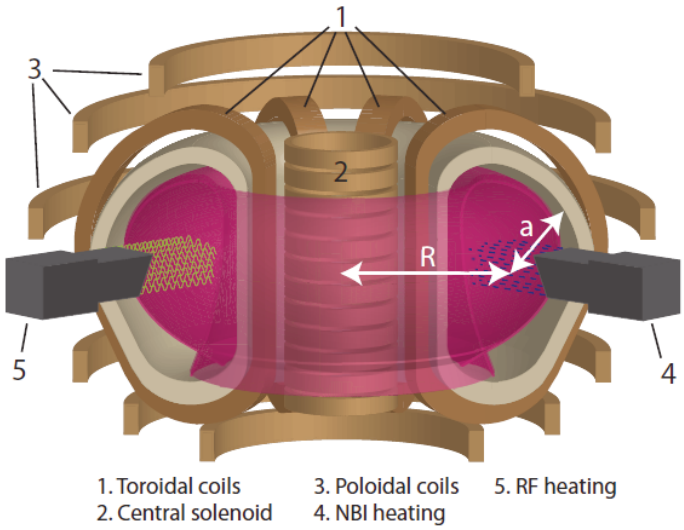

Figure 1. Schematic description of tokamak components.

Nuclear fusion is a reaction, where two light nuclei combine to form a heavier nucleus, and the binding energy of the system decreases. The difference of the internal energy is released as the kinetic energy of the product particles. Nuclear fusion for utilising in energy production means reaction between heavy isotopes of hydrogen, deuterium-deuterium (DD) and deuterium-tritium (DT) fusion which are described by the following reaction equations:

$$\mathrm{D} + \mathrm{D} \rightarrow {}^{3}\mathrm{He} + \mathrm{n} + 3.27\ \mathrm{MeV}$$
$$\mathrm{D} + \mathrm{D} \rightarrow \mathrm{T} + \mathrm{H} + 4.03\ \mathrm{MeV}$$
$$\mathrm{D} + \mathrm{T} \rightarrow {}^{4}\mathrm{He} + \mathrm{n} + 17.60\ \mathrm{MeV}$$
$$\mathrm{D} + {}^{3}\mathrm{He} \rightarrow \mathrm{p} + {}^{4}\mathrm{He} + 18.40\ \mathrm{MeV}$$

In the case of the first and last of these reactions, the produced neutron carries the majority of the released energy into the surrounding structures, from which it is to be harvested as heat into the primary cooling circuit and further for electricity generation.

Compared to U-235 fission, the cross sections are at least two orders of magnitude lower, as seen in Figures 2 [5] and 3 [6]. Therefore, if power densities practical for energy production are to be achieved, high temperatures and plasma densities have to be sustained over a reactor relevant time. Those key challenges are combined in the following simple criterion: the viable fusion reaction is defined by the fusion-triple product [7] with the relation

$$T_i \cdot n_i \cdot \tau_E \geq 10^{21}\ \mathrm{keV\,s/m^3}, \qquad (1)$$

where n_i ($\mathrm{m^{-3}}$) is the volume-averaged particle density, T_i (keV) is the ion temperature and τ_e is the confinement time of energy (s) defined as the ratio of the internal energy of the system and the input power.

In the current experimental devices of magnetic confinement, for instance the plasmas which have been modelled in this thesis, the achievable values for the density, temperature and confinement time are approximately 4-6·10^{19} m^{-3}, 8–10 keV and 100–150 ms, respectively. These quantities combine to triple product values in the range 6–8·10^{19} keV s m^{-3}. Such fusion relevant temperatures, typically more than 10 keV corresponds to 100 000 000 Celsius degrees**.** Hence, an increase in the triple product by 1—2 orders of magnitude is required in future devices to meet the aforementioned criterion for viable energy production.

Neutron transport and material effects in fission reactors are extensively studied and the analysis has become a mature and commercialised field almost everywhere in the world. The methods and analysis tools are sophisticated and widely used, so it is reasonable to bring this methodology into nuclear fusion applications. In fusion, there is no complex coupling between the chain reaction and heat transfer, which make the analysis of generated neutrons simpler than in fission reactors. However, the properties and behaviour of the fuel are extremely different: energy scale in the fusion plasma is from 1 eV to even a couple of MeV. Additionally, the fuel ions interact with a strong magnetic field, so a complete analysis of a fusion reactor as a power source requires combining many different fields of research: plasma transport modelling, fast particle analysis, neutron diagnostics, material research and power plant technology.

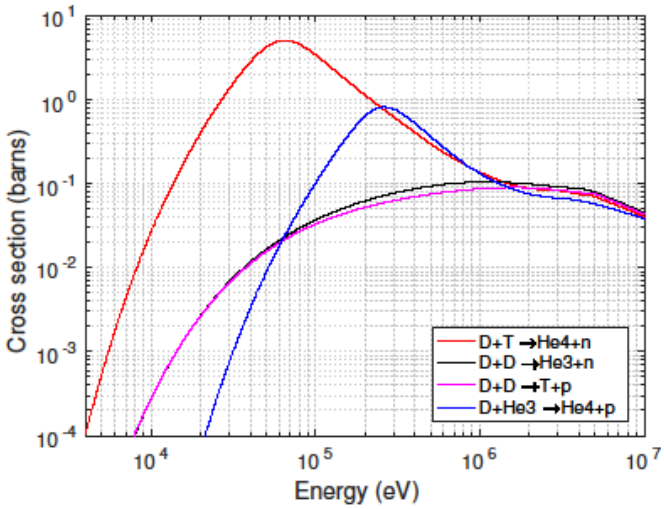

Figure 2. Fusion (DD, D^3He, DT) cross sections [5].

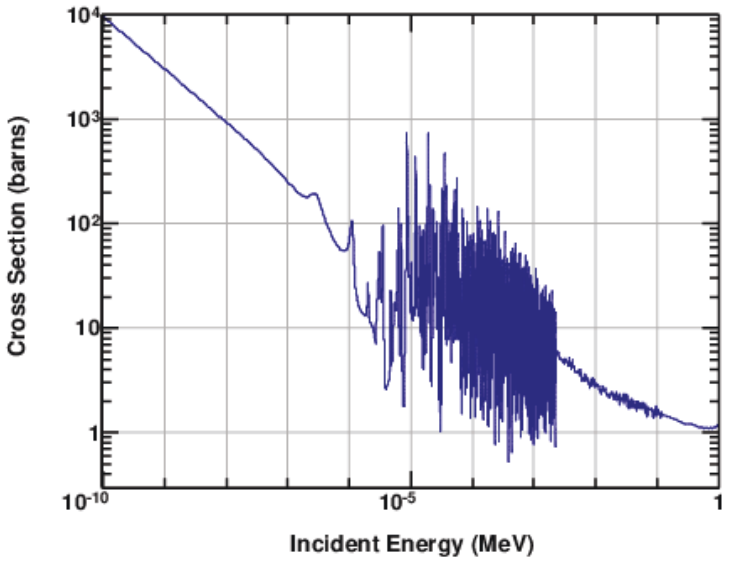

Figure 3. U-235 fission cross section [6].

1.2 Technical basis of magnetic confinement and tokamaks

European fusion research is focused on the concept of magnetic confinement and mainly tokamak type devices. The tokamak was developed by the Soviet scientists Tamm and Sakharov in the late 1950's [8]. In the tokamak concept, plasma is kept away from the vessel walls by strong magnetic fields. The equation of motion of a charged particle j in the electromagnetic field which constrains the motion of plasma particles as described below

$$\frac{m_j d\vec{v}}{dt} = q_j\left(\vec{E} + \vec{v}\times\vec{B}\right), \qquad (2)$$

where $\vec{E}$ and $\vec{B}$ are the electric and magnetic fields and $\vec{v}$, m_j and q_j the velocity, mass and electric charge of the particle j, respectively.

The solution of Equation 2, i.e. the orbit of the particle, is a helical line which is described in yellow in Figure 4, where the radius of the yellow helical orbit is the Larmor radius ρ_L defined as

$$\rho_L = \frac{m_j v_\perp}{q_j} \qquad (3).$$

The main components of a tokamak, illustrated schematically in Figure 1, are the torus-shaped (major radius R, minor radius a shown with white arrows) plasma chamber and the toroidal and poloidal coils for confining the plasma with strong magnetic fields. Additional but necessary components to the tokamak system are the particle sources and radio frequency antennas for heating, current drive and fuelling, diagnostic and measuring equipment and

the divertor for power exhaust and collecting the impurities and the helium reaction product or ash. [9]

It can be shown that the helical magnetic field in the torus (also presented in Figure 4) forms nested magnetic flux surfaces with constant pressure and is a combination of toroidal and poloidal components:

$$\vec{B}_{tot} = \vec{B}_{\varphi} + \vec{B}_{\theta} \qquad (4).$$

The toroidal component is produced by the toroidal field coils (see Figure 1), whereas the poloidal component is induced by the plasma current I_p. The plasma current is a fundamental part of the confinement and it is mainly produced by increasing the current in central solenoid. Usually, plasma current is defined as a toroidally directed current maintaining the confinement. It consists of different components

$$I_p = I_{ohm} + I_{bs} + I_{ext}, \qquad (5)$$

where I_{ohm} is produced with the mutual inductance principle with the central solenoid (can be seen in Figure 1), I_{bs} is the self-generated bootstrap current component driven by temperature and density gradients [10] and I_{ext} is produced as a result of fast particle current net effects [11]. In a continuously operating fusion reactor or long period pulses, the role of non-inductive components has to be significant since the inductive plasma current cannot be increased endlessly. They also affect the time evolution of other plasma parameters, such as the pressure and stationarity (see Section 2.2 for a more detailed description), so the current drive schemes have to be taken into account carefully in the estimation of confinement.

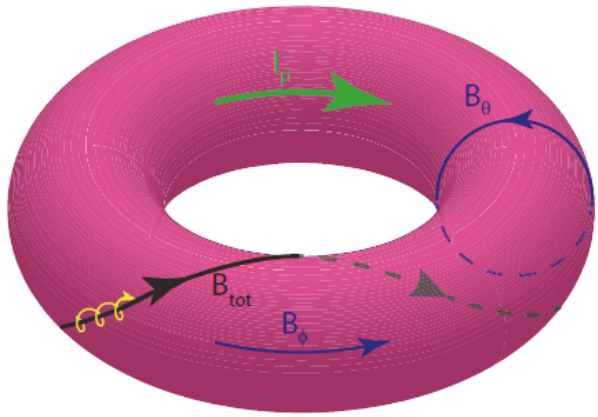

Figure 4. Magnetic field, current and particle orbits in the torus-shaped plasma

1.3 Concepts and definitions: plasma as a fluid or as particles

There are two principal methods for describing the physics of fusion plasmas: fluid equations or charged particle motion in an electromagnetic field. The first mentioned magnetohydrodynamical (MHD) fluid view can be used when the thermal Maxwellian component of plasma (characterised with the temperature and pressure of the electron or ion fluid) has a main role in the modelling. The model is valid when the large-scale behaviour of plasma during relatively long time intervals is analysed, for instance. The time scale here is typically some seconds, which corresponds to plasma pulse or phase length. In this thesis, the method is called *scenario modelling*, which means taking into account all physical or case-relevant effects, changing of the temperature, heating or plasma shape for instance, but utilising the toroidal symmetry, without going into details in particle interactions. [9]

Describing the plasma as a fluid can be started with the assumption of the MHD equilibrium or the equilibrium of the magnetic and kinetic pressure

$$\vec{J} \times \vec{B} = \nabla p, \quad (5)$$

where the magnetic anisotropy induces the pressure gradient for balancing the current density. Due to this equilibrium, the fluid quantities are constant on the flux surfaces and they can be presented with 1 (which means the circular cross section) or more generally with 1.5 dimensions in the case with more realistic elongated plasma cross section but simpler than fully 2 dimensional grid (see the comparison in Figure 9 in Section 2.2).

Generally used spatial 1.5 dimensional coordinate is the toroidally normalised ρ

$$\rho = \sqrt{\frac{\phi}{2\pi\ B_0}}, \quad (6)$$

where ϕ is the toroidal magnetic flux and B_o the reference field at the magnetic axis.

The components of the magnetic field can be solved with the curl of the poloidal field

$$\nabla \times B_\theta = \mu_0 j_\varphi = Rp' + \frac{FF'}{\mu_0 R}, \quad (7)$$

by using field in the flux functions ψ and $F = RB_\varphi$.

Modifying Equation 5 by writing the current density and magnetic field with the flux functions into

$$\frac{\partial}{\partial R}\frac{1}{R}\frac{\partial \psi}{\partial R} + \frac{1}{R}\frac{\partial^2 \psi}{\partial z^2} = \left(\mu_0 R \frac{\partial p}{\partial \psi} - \frac{F}{R}\frac{\partial F}{\partial \psi}\right), \quad (8)$$

gives is the most general description of the magnetic field in torus, called Grad-Shafranov equation. [12-13]

In contrast to the fluid description, the more detailed single particle view is used to study physical effects in a very specific field and small volume due to larger computing time which is required in particle following. In the particle view, the modelling means defining the distribution function of particles in the electromagnetic field by taking collisions into account. The

results from the particle following can be time and space-averaged and parametrised for using as a part of integrated (fluid) modelling. A typical example is modelling the behaviour of injected fast particles and taking the average fast particle distribution as a source term in the fluid temperature time evolution equation, which is described formally in Section 2.2.1.

1.4 Current and future devices

Currently, the largest and the most reactor relevant tokamak in operation is the Joint European Torus (R = 2.96 m, a = 1.25 m) in Oxfordshire UK [14]. It started operating in 1980's and executed successfully the first major tritium campaign in European tokamak device in the late 1990's, after small scale preliminary tritium experiments (PTE) in 1991 [15]. The scientific proof of fusion energy production in tokamak concept, equalling to energy gain of power as a fraction of produced and consumed power, Q=P_out/P_in =0.95 [16], was shown in those experiments. As can be seen in Figure 5, DT fusion neutron production is approximately two orders of magnitudes larger than a neutron production in DD reaction, so it is more suitable for reactor relevant plasma scenarios. The maximum neutron production rate was $5.7 \cdot 10^{18}$ neutrons per second (as seen in Figure 5) in the record plasma shot #42976 with DT mix 40/60 and it was achieved in the DTE1 campaign in 1997. Instead, in the DD experiments, the maximum neutron production with the current ITER-like-wall (ILW) plasma facing components was achieved at JET in 2016 experimental campaign.

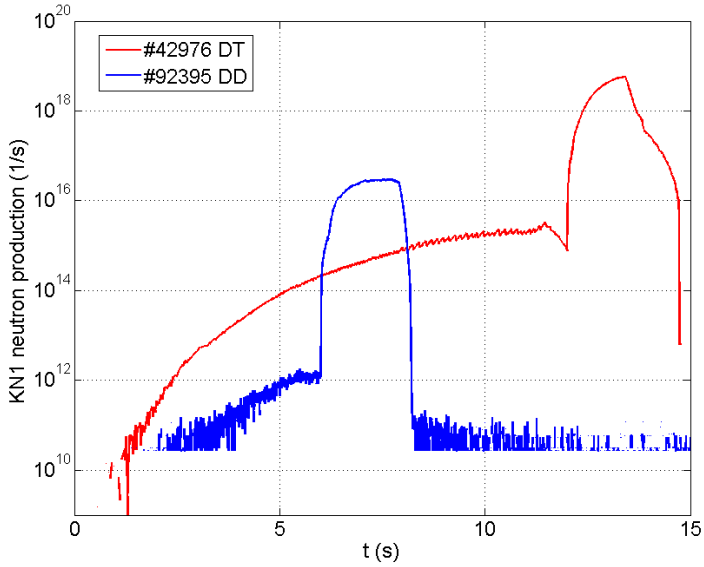

Figure 5. Neutron production in the record DT (#42976) and DD (#92395) in JET.

The next major step in fusion energy research is the construction of the ITER tokamak in Cadarache France as an international collaboration with China, EU, India, Japan, Korea, Russia and USA. Compared with existing devices, it will be massive: Radial dimensions are approximately two times larger than in current large tokamaks: the major radius will be 6.2

m and the minor radius 2.0 m and the fusion power 500-700 MW whereas in current devices it is around 15 MW [16, 17]. ITER will be started to operate in late 2020's in phases: the main goal of power multiplication factor Q=10 is planned to be achieved in five years from the first plasma and non-inductive steady-state plasmas will be studied a couple of years after that. [18]

Concluding the recent results of tokamak physics and engineering and the goals and requirements of ITER and other forthcoming reactor relevant tokamaks, the most significant technical challenges in forthcoming research are:

- Pulse-operating vs steady-state reactor
- Material effects and power exhaust
- Heating and fuelling
- Tritium breeding

Additionally

- Combining these and creating a fruitful interaction between the experts in several fields.

Construction and operation will be one of the largest technical challenges of humankind: the aim of ITER is to demonstrate the technical feasibility of fusion reactor for energy production. The success of this large and long-time-scale project, from designing to experiments by requires high quality and active research in existing devices. Before ITER operation, the research has to focus on the current devices. JET facilities have been upgraded several times to correspond to the ITER conditions and better functionality: NBI and ICRH systems have been enhanced to give about 30% higher power, fusion product diagnostics have better accuracy and the first wall material was changed from carbon to beryllium (main chamber) and tungsten (divertor) before the experimental campaign in 2012 [19, 20]. The next DT campaign is planned to take place in 2018-2020 when the main goals are to study tritium and D-T effects and test new relevant technological solutions before ITER operation. [14, 16-18]

Still, ITER is a scientific instrument and not a power reactor with a complete power plant construction connected to the power grid. For the demonstration of fusion power plant operation, the DEMO reactor [21] will be built with the experience from ITER operation. DEMO will be a complex system including the reactor primary and secondary loop and the electricity and automation systems licenced as a power plant. In this light, also balance-of-plant modelling needs to be integrated in fusion research for future applications.

1.5 Structure of the thesis

Production of fusion power will be maximised under reactor relevant conditions, which are characterised as a peaked ion temperature profile, high ion density and optimised fast particle population. However, fusion neutrons are not only a heat source but they also cause radiation effects and nuclear reactions in reactor and power plant materials. This thesis combines

two important fields in fusion research: it describes the modelling of reactor relevant plasmas as input for neutron transport calculation and balance-of-plant analysis.

First, the properties of reactor relevant plasmas in current devices have been studied with the general fixed tool box: integrated modelling suite of JINTRAC [22-27]. This section introduces the tools which are used in the modelling of plasmas as a heat and neutron source in reactor applications and presents a scan over different plasma parameters (Publication 1). In the second publication, a new tool AFSI ASCOT Fusion Source Integrator (Publication 2) for characterising fusion products is introduced. The third publication applies AFSI as a synthetic neutron spectrometer at JET tokamak (Publication 3) and the fourth publication describes AFSI-based neutron source as a part of total calculation chain (Publication 4) from the plasma fuel to the neutron related effects in reactor materials and power plant operation in future need.

The specific research questions formulated as:
RQ1: What is the sensitivity of the changing of plasma parameters in reactor relevant plasma operation?
RQ2: What is the neutron production and spectrum in different positions in the plasma? How can this be defined?
RQ3: What kind of interaction between plasma physics and neutronics is required in a complete analysis e. g. in activation or safety analysis?

2. Plasma scenarios

Current tokamak devices are pulse-operated due to the significant role of ohmic current driven by the toroidal field coils and therefore in the confinement. In the energy production applications, continuously operated reactors are required or alternatively, efficient energy storage techniques, such as the intermediate molten-salt circuit parallel to primary loop have to be available. However, maximising the self-generated component of the plasma current and achieving stationarity improve general efficiency.

Plasmas are characterised by the magnetic field, plasma current, temperature, density, shape and confinement time. The fusion triple product (defined in Equation 1) gives the lower limit of plasma parameters for net energy production, so increasing the confinement time gives the possibility to use lower density and temperature. Other quantities, which are used to compare plasmas, are dimensionless parameters: pressure fraction beta β, normalised Larmor radius ρ^*, normalised collisionality ν^* and safety factor q. They are used in the comparison of matching of plasmas in identity (same-size devices) or similarity (different size) experiments. Additionally, they make it possible to do prospects for the design of future devices, such as ITER and DEMO and new experimental schemes in current devices. [28-30]

In this thesis, the most relevant of them is safety factor q, which is the derivative of the toroidal flux respect to the poloidal flux by equation

$$q = \frac{d\phi}{d\psi} \approx \frac{r}{R}\frac{\varphi}{\theta}, \qquad (9)$$

which is approximately in the cylindrical geometry defined as ratio of magnetic field components scaled with torus radii.

Its derivative respect to the minor radius coordinate is the magnetic shear

$$s = \frac{r}{q}\frac{dq}{dr} \qquad (10).$$

The word “scenario” is used to characterise plasma types based on the heating, pulse length, current and efficiency. There are three generally used tokamak operational scenarios [31, 32] defined by values of q at $\rho = 0.95$ in the case of ITER

- pulse-operating baseline (BS) scenario defined by $q_{95} = 3$
- advanced hybrid (HY) or improved H-mode $q_{95} = 4$ [31-33]
- non-inductive steady-state or advanced tokamak (AT) scenario $q_{95} \geq 5$ [32-35]

In current tokamaks, the definitions are not so clearly fixed, so the parameters in Figure 6 can be varied in a slightly larger domain and the order of dimensional parameters is same in the same device. Confinement time, pulse length and beta are consistently larger in AT plasmas than in baseline for all devices. This looser definition is demonstrated in Figure 6 with typical parameters in ITER scenarios. The characterisation of scenarios is valid in all-size devices due to normalisation. Scenarios can be classified also with the shape of the q profile and the magnetic shear. The baseline scenario represents typical plasma in high confinement mode (H-mode) with an edge transport barrier (ETB) [36]. ETB is a well-defined region with a strong local pressure (or temperature and density) gradient and supressed anomalous transport in this region which is necessary in reactor applications. Otherwise, the properties in baseline plasmas are not reactor relevant and suitable for tokamak-based fusion power plants. For example, stationary phases are quite short due to the high fraction of ohmic current component which is based on the induction.

Advanced tokamak scenarios can be defined by high fusion efficiency with operation close to steady state conditions [31], which indicates optimised heating and current alignment (quality and shape of the current profile) and longer pulse length. In addition to the reverse-shaped q-profile or a negative magnetic shear, the current density profile is different compared to baseline plasmas. This scenario can be very important for studying the steady-state operation of forthcoming fusion reactors targeting to suppress the plasma turbulence and leading to enhanced confinement since, retaining the reverse shape of the q profile is connected to triggering an internal transport barrier (ITB, defined like ETB but located on the half radius) [37, 38] which decreases turbulence and improves confinement [39]. Although the ITB triggering is a widely studied topic, the mechanism is not well understood and for example, ideal results from the triggering of the density ITB have not been achieved in JET tokamak [38, 40].

The hybrid scenario is not so clearly defined than baseline or advanced scenario. The main purpose for the development of this scenario is to take the benefits from AT and BS scenarios but to minimize the difficulties to reach an acceptable compromise. The hybrid scenario is not targeting a pure non-inductive current and steady-state operation but it gives better confinement and fusion efficiency than the baseline scenario.

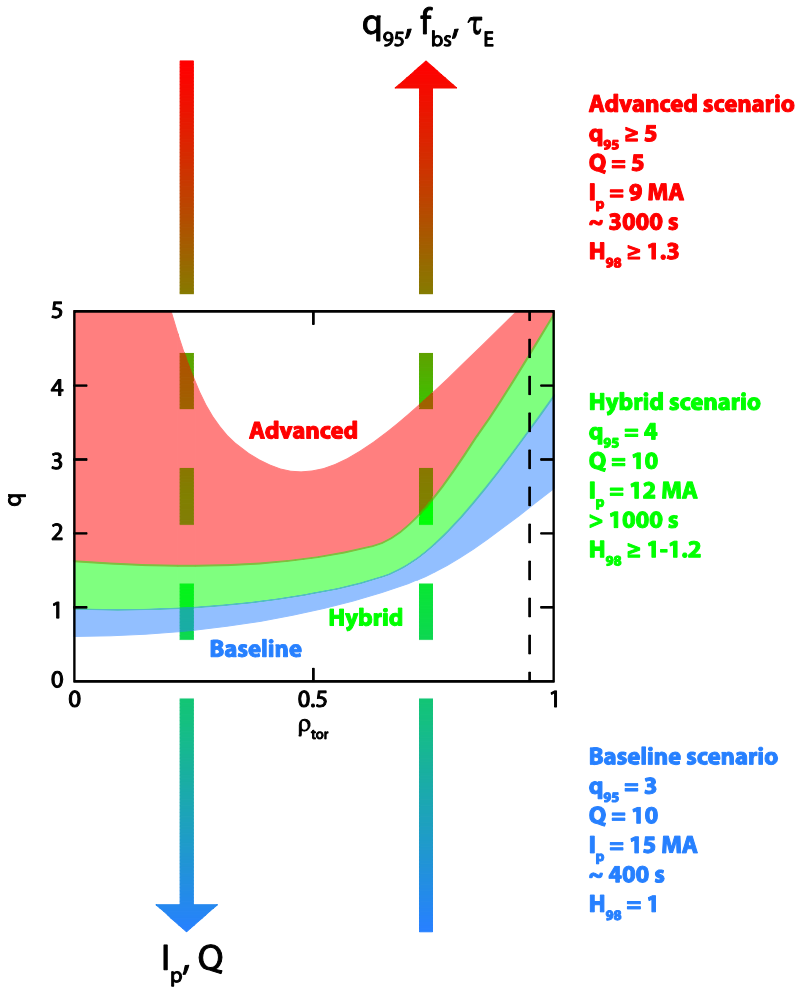

Figure 6. Characterisation of the plasma scenarios based on the shape of *q*-profile.

Due to different sizes and technical properties (such as heating systems and chamber) of devices, physical phenomena can be compared with dimensionless parameters. The quality of confinement can be described simply by the ratio of kinetic to magnetic pressure, the dimensionless parameter beta

$$\beta = \frac{2p}{\mu_0 \ {}_0{}^2} \quad (11).$$

Commonly used poloidal beta is defined with the poloidal component of magnetic field. It is connected to the poloidal current density and self-generated bootstrap current [10, 41, publication 1] which is discussed in Subsection 2.2.2

The normalised Larmor radius (compare Larmor radius in Equation 3)

$$\rho_{*,j} = \frac{\sqrt{T_j m_j}}{q_j a} \quad (12)$$

is proportional to $\sqrt{T}$, so it compares temperature and characterises particle radii in different plasmas and neoclassical transport coefficients when the radii is normalised respect to minor radius and the magnetic field of the selected tokamak.

The normalised collisionality is connected to the collision frequency and interactions between particles and it is defined by

$$\nu_{*,j} = \left(\frac{R_0}{r}\right)^{3/2} qR\nu_{ei}\sqrt{\frac{m_j}{2T_j}}, \quad (13)$$

where R_0 and r are major and minor radial coordinates which go from the central or magnetic axis to the plasma boundary. Electron-ion collisionality ν_{ei} describes the impact of the electron collisions with the ions. Collisionality, or collision frequency, characterises the diffusion coefficient ($\chi = {\rho_L}^2\nu$) with the Larmor radius, so it has an important role in transport analysis and via q ($\sim {}^1/_{I_p}$) and radial coordinates it takes into account also the fixed dimensions of the plasma and the shape of the current profile.

Dimensionless parameters in the reactor relevant AT plasma are illustrated in Figure 7. The normalised Larmor radius and collisionality were matched very well in these identity experiments in JET and JT-60U but the beta is peaked in JT-60U due to a strong density ITB. [42, 43]

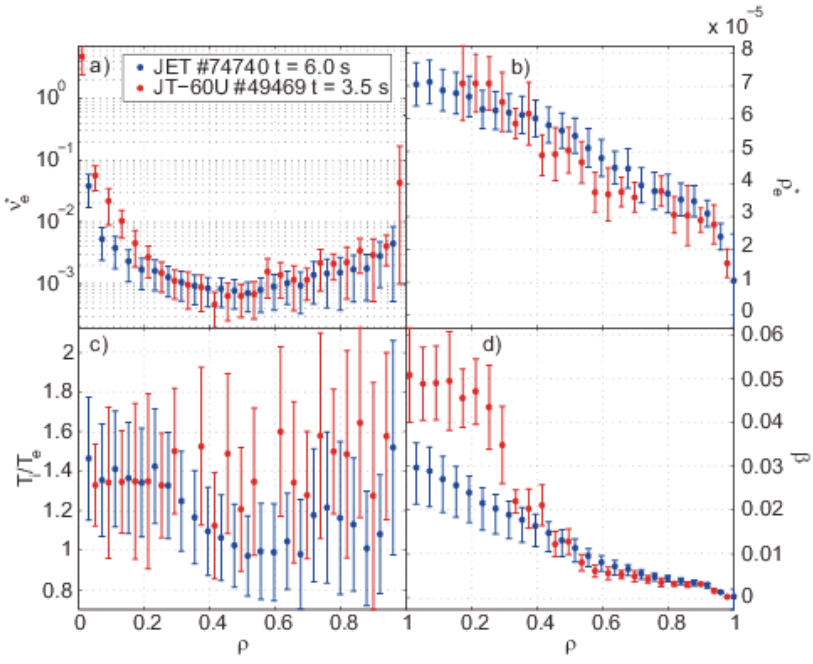

Figure 7. Dimensionless plasma parameters $\nu, \rho, \frac{T_i}{T_e}$ and β as function of toroidal ρ in JET and JT-60U tokamak in AT plasmas. (Publication 1)

2.1 External heating and current drive

Magnetically confined plasma is mainly heated by high energy neutral particle injection (NBI) and resonances of radio frequency waves with plasma ions (ion cyclotron resonance heating ICRH) or electrons (electron cyclotron resonance heating ECRH) and in addition there is also a minor contribution from ohmic heating. These systems are also used for driving non inductive plasma current and NBI provides additionally a particle source. As an example of current large-size tokamak, JET has two NB injectors and two ICRH systems (including ITER-like antenna and four A2 antennas), NBI having the most significant role in the heating. Usually NBI covers approximately 80% of all external heating and it is essential especially in hybrid and advanced tokamak scenario experiments where higher external power is required. In this thesis, plasma heating is considered as a mathematical source terms in the transport equation (power, particle or current source) or as a contribution in the input data without detailed technical information. [44, 45]

The NBI consists of an ion source, a particle accelerator, a neutraliser and a deflector magnet. In general, the whole NBI system of a tokamak includes several particle sources, called PINIs (positive ion neutral injector, used in current devices), directed to the plasma with the different values of angles ϕ and θ. For example in JET, the NBI system includes two NB boxes which both have eight PINIs with different but fixed angles ϕ and θ. Half of the PINIs are tangential-like and half normal-like directed. The absorbed power depositions and contribution to the total plasma current depend on the directions of the PINIs which are presented in Figure 8. Normally-directed (or on-axis with respect to the magnetic axis) neutral beams give the heating power but the contribution to the toroidal plasma current is low. Instead, the tangential beams (off-axis) can produce a significant part of the non-inductive current. By changing the angle θ, the on/off-axis current components can be controlled but usually the angles are fixed in maintenance and they are not changed or re-directed shot by shot. [46]

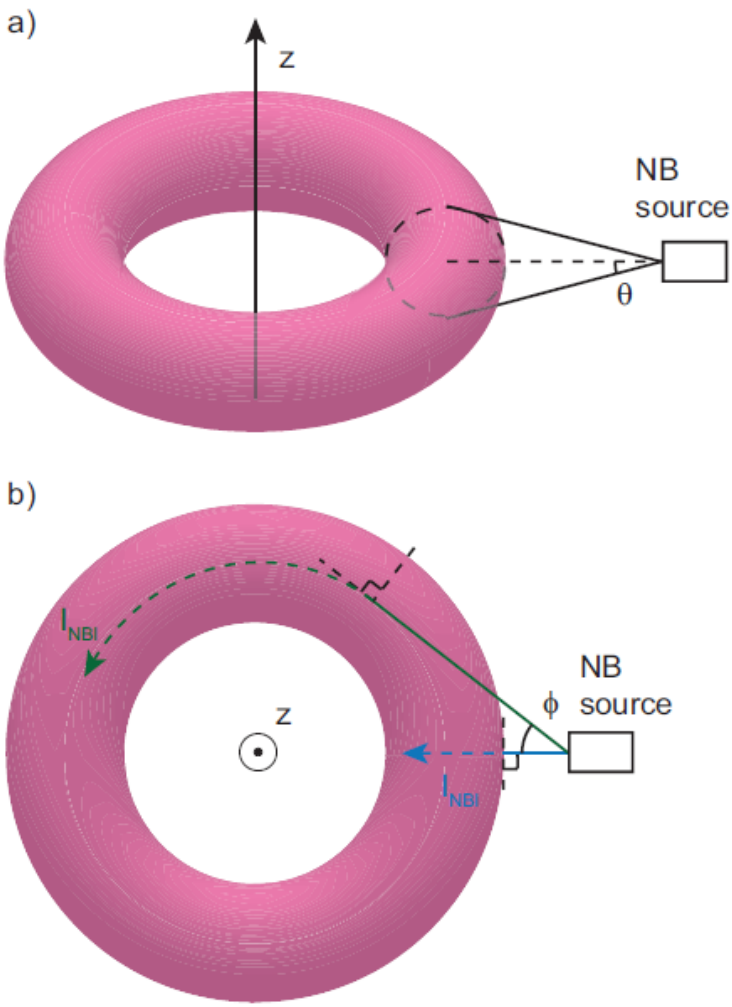

Figure 8. Schematic view of NBI system alignment.

While NBI is usually the main heating method at JET, also ICRH has many beneficial properties. The resonance occurs in the locations in which the wave frequency equals the Larmor frequency of the heated species

$$f_L = \frac{q_j}{m_j}, \quad (14)$$

which is called the first harmonic or fundamental heating. Additionally, if the multiplications (second harmonic etc.) of the Larmor radius are used, the scheme is called the multiple harmonic heating. The resonance frequency depends on the magnetic field which varies along the major radius. This makes ICRH suitable for localised heating in a desired region in the poloidal cross section. Energy transfer from the radio wave to the plasma particles is connected to the frequency multiplication in a complex way: main thermal plasma ions are heat-

ed inefficiently by fundamental heating. Thermal minority particles, such as hydrogen in deuterium plasma can be heated effectively by fundamental frequency whereas energetic minority particles are heated with the multiple harmonic schemes. ICRH heating is not similarly connected to the mechanical settings of the system but rather by the properties of the antenna. [45, 47]

2.2 Integrated modelling – tools

Integrated modelling can be defined as the modelling of the plasma scenario (including temperature, density, geometry, heating and current drive) by combining different phenomena in different scales. In this thesis, the integrated (core plasma) modelling consists of the effects in core plasma. The grid of modelling spans the toroidally axisymmetric plasma from the central axis to the last closed magnetic flux surface, in other words: it is defined from 0 to 1 in toroidally normalised rho coordinate.

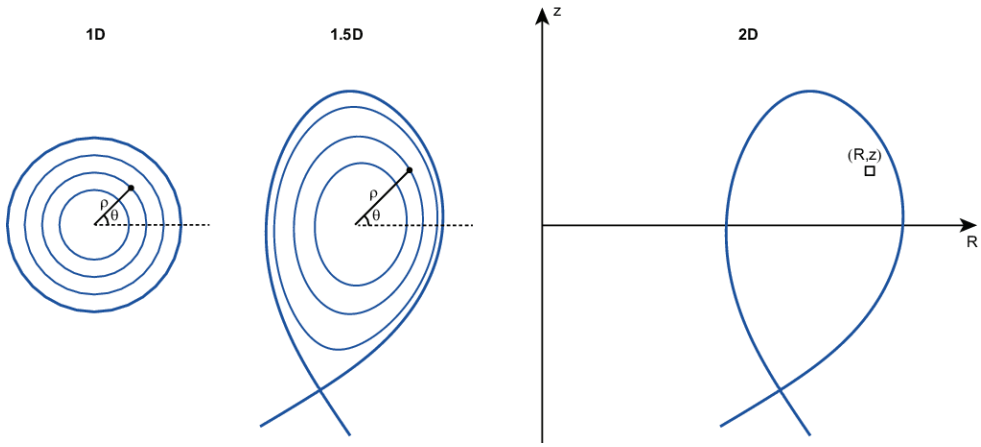

Figure 9. Modelling grid in the 1D, 1.5D and 2D poloidal cross section.

2.2.1 Plasma transport equations

Plasma transport is a combination of classical, neoclassical and anomalous components. By viewing a general form of the continuity equation for quantity X

$$\frac{\partial X}{\partial t} + \nabla \cdot \Gamma = Sources - Sinks. \qquad (15)$$

where the flux Γ is described by a general 1 or 1.5D transport equation

$$\Gamma = \chi \nabla X + sources - sinks, \qquad (16)$$

where χ (or called D generally in particle diffusion case) is the diffusion coefficient and ∇X the gradient which drives the flattening of the differences.

The classical component of χ includes the classical collisions of the particles and the neoclassical approach is corrected by effects due to the toroidal geometry. In the other words: The classical mean free path is the Larmor radius (see the Equation 3) whereas in the neoclassical view it is changed to

$$\Delta x_{neo} = \frac{\rho_L^2 q^2}{\varepsilon}, \qquad (17)$$

where ε is the inverse aspect ratio, a/R. This neoclassical mean free path is called the banana width, hence the fraction ε of the particles are trapped on the banana-shaped orbits [9, 48, 49]. Classical and neoclassical mean free paths are compared in Figure 10.

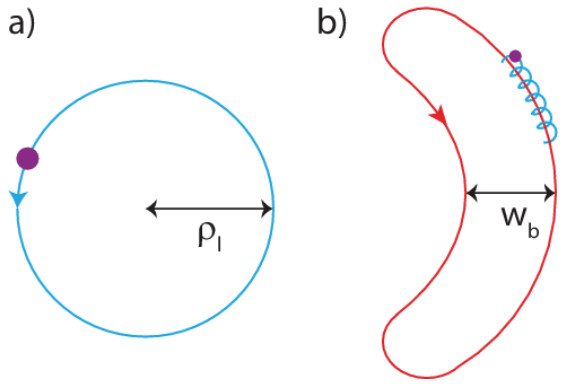

Figure 10. Classical (a) and neoclassical (b) mean free paths presented with the particle orbits.

Due to different masses, the neoclassical mean free path is about 100 times larger for ions than for electrons when the temperature is the same. However, the anomalous component, driven by turbulent processes, dominates transport normally in all channels, and only in few cases the neoclassical transport is significant:

- Current diffusion is a purely neoclassical effect, excluding some magnetohydrodynamical instabilities.
- In transport barrier regions, when the anomalous component is totally or partly supressed [36-37]
- In impurity transport, the neoclassical mean free path is sufficiently large due to the larger mass of particles as due to the connection $\chi_{neo} \sim \rho_L \sim m_j$. [48, 49]
- Close to the magnetic axis excluding of sawteeth [50]

Transport barriers are defined as a local suppression of anomalous transport. Transport effects are coupled and they can be presented in a matrix form

$$\begin{pmatrix} /n \\ \Gamma_e/(nT_e) \\ \Gamma_i/(nT_i) \\ j_\varphi \end{pmatrix} = \begin{pmatrix} \boldsymbol{D} & 21 & 31 & 41 \\ 12 & \boldsymbol{e} & 32 & 42 \\ 13 & 23 & \boldsymbol{i} & 43 \\ 14 & 24 & 34 & \end{pmatrix} \begin{pmatrix} n/n \\ T_e/T_e \\ T_i/T_i \\ E \end{pmatrix} \qquad (18)$$

Where diagonal terms describe the general diffusion part and non-diagonal terms are convection, sources and sinks. The first equation describes the particle diffusion, the second and third ones the heat diffusion for ions and electrons and the fourth one current diffusion. [51]

2.2.2 Current diffusion and bootstrap current in reactor relevant plasmas

The plasma current and its time evolution have an important role in advanced scenario plasmas, because there is the objective to sustain the reversed shape of q profile by due to positive gain to the self-generated plasma current [10, 52, 53]. As mentioned, current diffusion is a neoclassical phenomenon which can be derived starting from Maxwell's equations, in particular the curls of the electric and magnetic fields in the time-varied case. The current diffusion equation is written with the source terms in the form

$$\nabla^2(\eta \vec{}_{ohm}) = \mu_0 \nabla^2\big(\eta(\vec{}_{tot} - \vec{}_{d} - \vec{}_{bs})\big) = -\mu_0 \frac{d}{dt}(\vec{}_{tot}), \qquad (19)$$

where η is the neoclassical resistivity (compare to the conductivity in the matrix diagonal in Equation 18). Externally produced current density j_{ext} driven by NBI or RF-heated particles is an external source term in the equation and the other source term, j_{bs}, is the self-generated bootstrap current density. It is an internally generated neoclassical effect by temperature and density gradients.

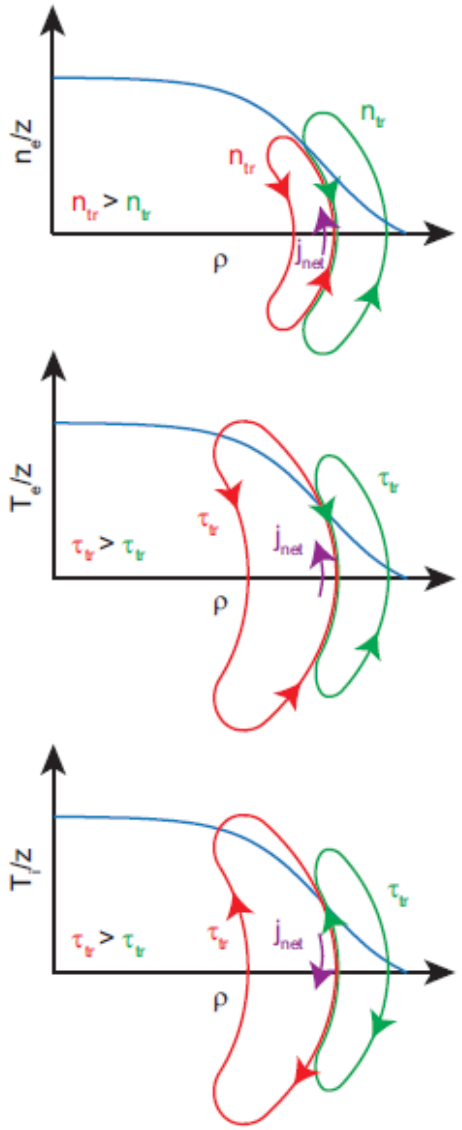

Figure 11. The forming of banana current by trapped particles due to density and temperature gradients

Generating bootstrap current can be demonstratively explained with a simple linear approximation. Based on the neoclassical theory, the fraction of banana trapped particles is equal to the square root of inverse aspect ratio $\sqrt{\varepsilon}$ so with the density of total amount of trapped particles is $n_{tr} = \sqrt{\varepsilon}n$. Trapped particles cause so called banana current around the banana orbit, but when density gradient exists, there is a net effect current between two bananas which is demonstrated in Figure 11. Correspondingly, temperature gradients cause the same effect in the energy or velocity (parallel velocity on the banana edges). This net current is defined by

$$j_b = q_j(\ n_{tr} \cdot v_{\|} + n_{tr} \cdot\ \ v_{\|}) = q_j w_b \varepsilon \left(\nabla n \cdot \sqrt{\frac{2T}{m}} + \nabla T \cdot \frac{n}{\sqrt{2mT}} \right), \qquad (20)$$

where the parallel velocity has been assumed as

$$v_{\|} = \sqrt{\varepsilon} v_{th} = \sqrt{\frac{2T\varepsilon}{m}}, \qquad (21)$$

where v_{th} is the averaged thermal velocity. When the net current effects from both, electrons and ions are combined, a good approximations for the self-generated bootstrap current is got as [50]

$$\overrightarrow{\ \ bs} = \sqrt{b} \frac{R}{0} \left(2.44(T_e + T_i) \frac{dn_{tot}}{d\psi} + 0.69 n_{tot} \frac{dT_e}{d\psi} - 0.42 n_{tot} \frac{dT_i}{d\psi} \right), \qquad (22)$$

where $b = (B_{max} - B_{min})/(B_{max} + B_{min})$ describes the inhomogeneity of the magnetic field and $\sqrt{b} B_{\varphi}/B_0$ the same geometrical effect as $\sqrt{\varepsilon}$ in the banana current approximation. [48, 49, 52, 53]

The other important neoclassical quantity is the current diffusion coefficient, resistivity, which is defined by

$$\eta = \frac{m_e \langle \nu_{ei} \rangle}{n_e e^2}, \quad (23)$$

where $\langle \nu_{ei} \rangle$ is the volume-averaged electron-ion collision frequency (introduced with the collisionality in Section 2). Now it can be seen that based on the numerical coefficients of the gradients in Equation 22, the electron density and temperature have the most significant effect to the current diffusion. [54]

Increasing the electron temperature decreases the current diffusion and increases the bootstrap current density. However, the effect of the pressure gradient to drive the bootstrap current can be also increased or decreased by the current flux function *F* [40, publication 1], which can be seen from the connection between *F,* poloidal current density and poloidal beta [28, 40, 55]. Transition from the diamagnetic to the paramagnetic state is given by

$$F' = \frac{\mu_0(-R j_{\varphi} + p')}{F} = 0. \qquad (24)$$

The bootstrap current density can be written as

$$j_{bs} = \xi - \varepsilon^{1/2} R p \qquad (25).$$

where ξ is the difference between the real bootstrap current density and the pressure gradient approximation. By using equations 24 and 25, the bootstrap fraction and the bootstrap current density are

$$\frac{j_b}{j_{\varphi}} = \frac{-\varepsilon^{\overline{2}} R p' + \xi}{-R p' + \frac{FF'}{\mu_0 R}} \Rightarrow j_{bs} = \frac{\varepsilon^{\ /2} \left(\frac{-\xi}{j_{b\ ,approx}} + 1 \right)}{\left(-\varepsilon^{\overline{2}} \left(\frac{-\xi}{j_{b\ ,approx}} + 1 \right) + 1 \right)} (j_{ohm} + j_{\ d}) \equiv j_{bs}^{\ rit}. \qquad (26)$$

This condition describes decreasing (diamagnetic state [9]) or increasing (paramagnetic [9]) the effect of the pressure gradient in bootstrap current formation. The same gradient does not cause the same current in all or even same-size devices with similar plasmas but it has a strong connection to the geometrical features via the inverse aspect ratio, which can be seen in the improved formula of the criticality condition, which is presented in the first publication:

$$j_{bs}^{\ rit} = \frac{\varepsilon^{\overline{2}}\left(1-\frac{\xi}{j_b-\xi}\right)\left(\frac{E\varphi}{\eta}+j_{ext}\right)}{\left(1-\varepsilon^{\overline{2}}\left(1-\frac{\xi}{j_b-\xi}\right)\right)} \leq j_{bs}, \qquad (27)$$

When the condition of critical bootstrap current is valid, the stationary state (defined by zero time derivatives) can be achieved. In Publication 1, satisfying this condition in JET and JT-60U has been studied in the experimental data input and also in the sensitivity tests where different parameters, density and geometry mainly have been scanned in current diffusion simulations which have been introduced briefly in the next subsection.

2.2.3 Modelling of fast particles – ASCOT

The behaviour of fast particles is different from the thermal main plasma due to different radii of orbits, reaction probabilities and collision times. Additionally, the population of fast particles is located to the smaller region in the poloidal cross section, so utilising poloidal axisymmetry is not generally accepted way to make analysis simpler. For this reason, kinetic Monte Carlo based particle following is the mostly used approach for fast particle studies.

ASCOT [56, 57] is an orbit-following Monte Carlo code that solves the distribution function of fast particles in tokamak or stellarator plasmas. In the code, a set of test particles representing the fast ion source is followed and their distribution is collected as the particles slowing down. For NBI particles, the source is calculated using the BBNBI [58] code which calculates the ionisation profile by following test particles from the injector until they are ionized in the plasma. A simple work flow of the ASCOT procedure is presented in Figure 12.

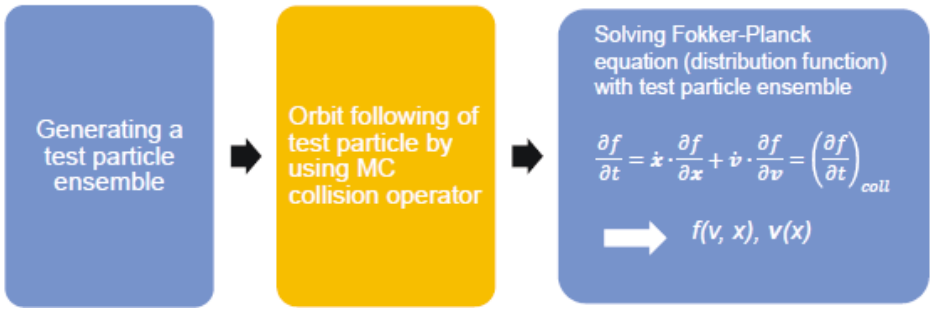

Figure 12. ASCOT work flow

2.2.4 JINTRAC coupled codes

JINTRAC (JET Integrated Transport Code) [22, 23] is a simple-to-use coupled code system including the tools for modelling the whole plasma scenario from the core plasma to the wall,

including SOL/divertor, and plasma-wall interaction. It consists of several modules including NBI or RF heat sources, equilibrium solver, particle sources from fuelling and recycling, impurities, diffusion coefficients and reaction product calculation. The core module JETTO [24-27] solves the transport equation matrix in concurrent interaction with other coupled codes.

In the case of solving the current diffusion equation and stationarity, the following modules are used: ESCO analytical equilibrium solver, ASCOT for the source term due to NBI particle current, NCLASS [58] for neoclassical resistivity and bootstrap current source. This interactive procedure is presented in Figure 12 which shows also the (experimental data-based) inputs which are required for self-consistent analysis.

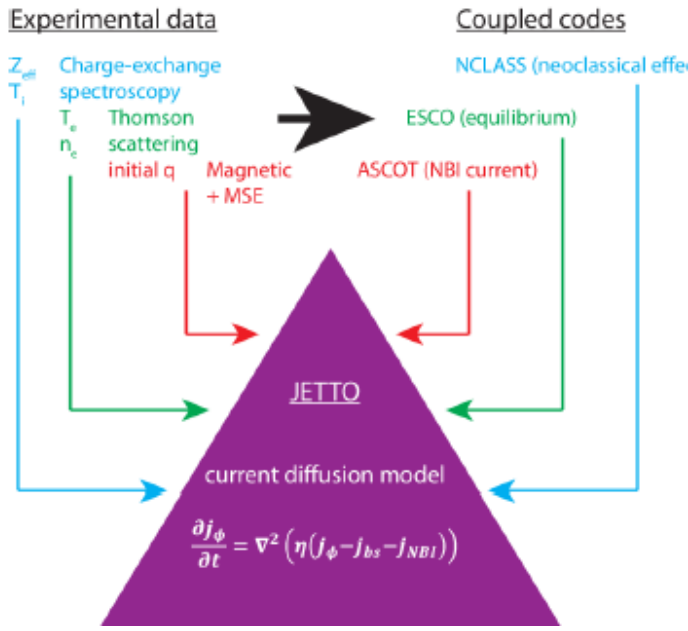

Figure 13. Interaction between JETTO and coupled codes in the JINTRAC integrated modelling system.

2.3 Reactor relevant plasmas

Two significant features in reactor relevant plasmas in tokamak concepts are maximising the neutron production and providing conditions for steady-state operation. In current DEMO scenarios, the reactor will operate by long-time pulses, which means timescales of hours. Between pulses, power generation is sustained by transferring heat from the molten-salt heat storage to the power plant secondary loop circuit. During discharge, part of the reaction heat is charged to the molten-salt tank. Steady state operation requires generating plasma current non-inductively but also increasing the non-inductive current fraction in pulse-operated scenarios increases the general efficiency of the plant. [21]

Maximising the fusion power and neutron production is strongly connected to the ion temperature via reaction cross section [5]. Another significant parameter is the total plasma volume. Very small variations in the plasma geometry or the shape of the poloidal cross sections affect strongly the total neutron production.

Table 1: Comparison of the plasma parameters in JET and ITER baseline and advanced tokamak scenarios [17, 55].

parameter	JET baseline #92440 (2016)	JET advanced #74740 (2008)	ITER baseline	ITER steady state
B_t (T)	2.0	2.2	5.3	5.3
Ip (MA)	2.1	1.5	15	9
T_e (keV) max	3.2	6.7	25	24
n_e (10^{19} m^{-3}) max	7.5	3.4	10	7
$P_{tot,ext}$ (MW)	11.3	13	73	110

The goals for the ITER steady-state scenario include the requirements for a high beta and non-inductive current fraction (self-generated bootstrap fraction >50% and the rest replaced by externally driven current) [18, 59]. Strong pressure gradients are necessary in good confinement and higher non-inductive fraction by driving sufficiently large internally-generated current, but they have not been fixed in the ITER work plan based on the recent results from the studies on current tokamaks.

The most recent identity plasma experiments in large tokamaks were done in 2008 at JET and JT-60U to study different confinement properties and current profile time evolution in AT scenarios [42, 43]. These were the first experiments where the global plasma parameters and profiles were matched between two similar-sized tokamaks in AT plasmas with reverse q and high bootstrap fraction.

Experimentally, both dimensionless parameters and plasma profiles were successfully matched in the initial state, but the time evolution of the q-profile and electron density was different. Based on the current diffusion modelling (including source terms j_N and j_{bs}) results presented in Publication1, significant differences between these two experiments have been characterised, in addition to the fixed properties of the devices: NBI alignment, total plasma current and plasma geometry [43].

The most important results from the analysis in Publication 1 are presented in Figure 14. The neoclassical bootstrap current density presented from the current diffusion simulation based on purely experimental data profiles (black solid line) and required bootstrap current density for the transition where the effect of the pressure gradient on the bootstrap current drive has a positive gain. Blue (JET) and red (JT-60U) cases are the corresponding simulations but the replaced electron density profiles were used. In the JT-60U experimental case the critical current condition is sustained and also the level of critical current density is lower. This can be observed even in the electron density profile without the ITB, where the same density gradient produces two times more bootstrap current in JT-60U than in JET.

The role of the plasma geometry is significant not only for total fusion power but also for achieving stationarity. Based on the sensitivity tests reported in Publication 1, changing geometrical features (elongation, triangularity, inverse aspect ratio) is a more efficient way to increase the bootstrap fraction and decrease the level of critical bootstrap current density compared to the electron ITBs. Beneficial geometry (high inverse aspect ratio ε and triangularity), which has been obtained in JT-60U, is strongly connected to the positive gain of negative pressure gradients. This can be seen in Equation 25 for bootstrap current when the critical level of bootstrap current has been achieved.

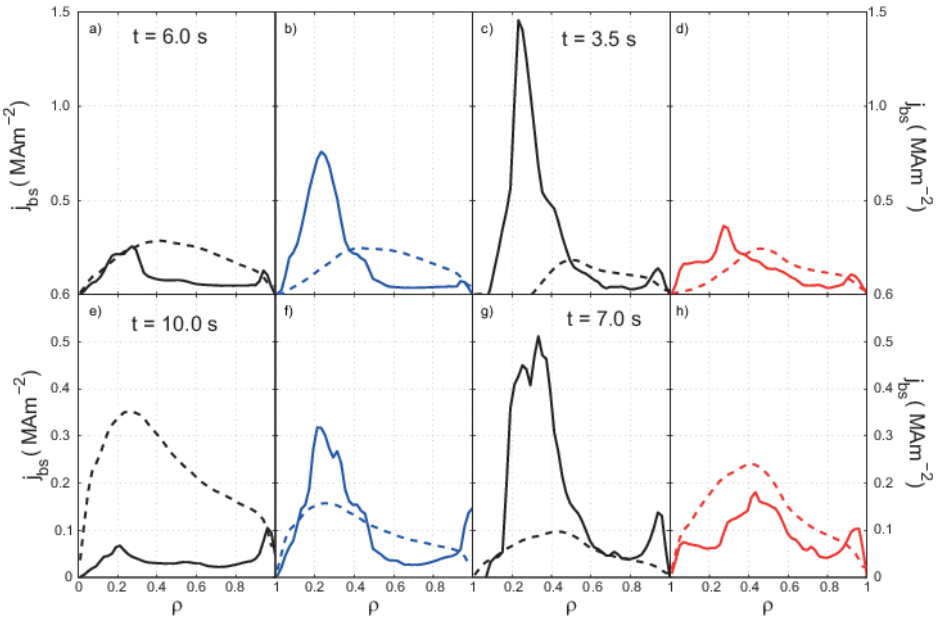

Figure 14. Bootstrap current density from NCLASS (solid) and critical bootstrap current density (dash) in JET and JT-60U. a),e) Simulation with experimental JET data c),g) Simulation with experimental JT-60U data b),f) JET simulation with JT-60U electron density d),h) JT-60U simulation with JET electron density. (Publication 1)

The most promising results in AT scenarios have been achieved in JT-60U in the early 2000's and the achieved results compared with ITER goals are presented in Figure 15. In those experiments, high poloidal beta, bootstrap fraction and H factor [18] exceeded the ITER target values [38]. These indicate improved confinement with higher temperatures and densities, better efficiency and neutron production. In contrast, the fuel purity was the farthest from the ITER goal – only 2/3 of the target value [60]. Fuel purity and impurity accumulation will be problematic issues in developing of the AT scenarios with transport barriers, due to impurity accumulation in the core plasma.

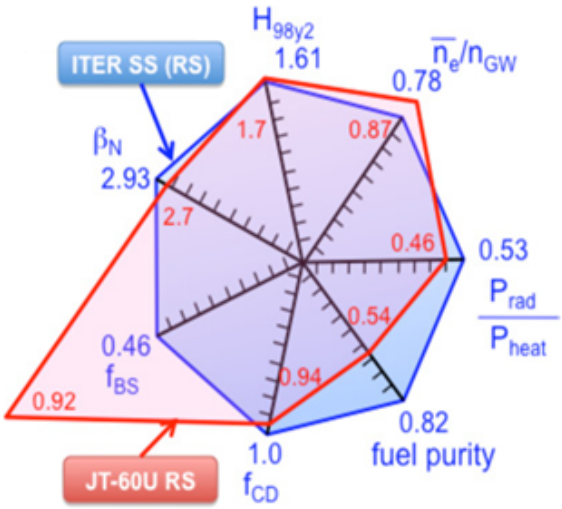

Figure 15. JT-60U record results compared with the ITER goals [35].

There are no the AT scenario experiments planned during the first operational years of ITER [61]. However, AT scenarios can provide a feasible solution for power plant applications and are planned in ITER in the 2030s [62-64].

3. Fusion products

3.1 Plasma as heat source

The main part, 80%, of the energy in a fusion device is transferred out by neutrons. The rest of the energy is carried

- As an isotropic radiation
- convectively with the high energy alpha particles to the chamber walls
- by migration to the divertor plates via thermal particles by convection.

The modelling of the heat source is important, not only for the design of the heat transfer system, but also it has to be taken into account due to safety aspects: high neutron fluxes cause activation in the reactor materials.

Typically, in thermo-hydraulic system modelling, the heat source is described only by parametrisation based on produced power but the physical effects in the plasma fuel and materials are not included. However, the response time and the secondary reactions have a significant effect on the total power production. In coupled thermo-hydraulic modelling, the heat source is described starting from the neutron producing reactions in the plasma fuel. The neutron source is given to the neutron transport module which calculates the real neutron flux through the cooling elements and takes into account the secondary reactions and gamma production which can also cause the damage in surrounding materials. This coupled modelling framework is described in more detail in Section 5.2.2 in balance-of-plant.

3.1.1 Fusion neutrons

The principle of the modelling of neutron and gamma transport in materials is mainly similar for the neutrons produced by fission or fusion reactions. However, the effects in materials are different due to energy spectrum of neutrons. Typically, the energies of neutrons produced in fission reactions are around 2 MeV whereas in DT fusion, the major part of the neutrons are born with an energy around 12-16 MeV. Even in DD fusion, the energy is of the order of magnitude 2-3 MeV, which enables more threshold reactions and longer mean free paths for neutrons in the materials. In addition, the materials in fusion devices are different, so various reactions which are not relevant in fission reactors, are observed in fusion applications.

Fusion reactions which produce neutrons can be divided to several groups based on the energy or source of reactive particles. Typically, the three following groups are used:

- thermal particle reactions,
- thermal-fast particle reactions and
- fast particle reactions.

The first group (called thermal in this case) consists of the reactions between thermal deuterium and tritium ions which can be described as a fluid (with one ion density and temperature) with a Maxwellian distribution when the fuel fraction 50/50 is assumed. The energies of the particles in this group are typically up to 20 keV. The second group (thermal-fast) includes reactions between thermal and fast particles created by neutral beam injection or RF heating. Their energies cover the interval from 50 keV to 2 MeV depending on the heating system: for example, in ITER NBI system particles are planned to be 1 MeV deuterium ions [18]. The third group includes the reactions between fast particles from the same or a separate source. This classification is computationally beneficial hence every group can be presented representatively with separate distribution functions each source. Neutron source codes, including calculation of the production rate and spectra are generally used in several applications: neutron source and synthetic diagnostics are mentioned as the most significant of them. The mostly used analytic tools are parametrised simplified sources or codes which are based on the Maxwellian distribution. They are mainly used to calculate the thermal contribution or average production especially in large devices such as ITER and DEMO. Instead, Monte Carlo codes, for example ControlRoom [65] and DRESS [66], are used in more detailed analysis and they can be extended also to gamma production such as GENESIS [67, 68]. In the computational source, NBI, RF and heat transport codes can be coupled to the neutron source routine which enables also time dependent neutron sources and considers all reaction types.

In current devices, with the exception of the DT campaign in JET, significant part of the neutron yield is produced in DD reactions between fast and thermal particles. Production rates in different reaction types in JET are presented in Section 3.2 as a validation case of AFSI ASCOT Fusion Source Integrator (in publication 3). Those figures show that all reaction types contribute significantly to the total production rate and they are required at least in the validation of computational methods. In forthcoming reactor-relevant tokamaks, thermal reactions dominate the neutron production due to the smaller fraction of fast particles. However, thermal-fast and fast particle reactions can be significant due to the different energy spectra of the emitted neutrons. The highest energies of neutrons are achieved in the reaction between two RF accelerated particles. Additionally, in thermal-fast and fast particle reactions, the velocity distribution is strongly asymmetric on the poloidal cross section, which has been illustrated in the forthcoming Figures 19 for JET and 27 in Section 5 for ITER.

In the general, the neutron production in the reaction between particles 1 and 2 can be defined by the equation

$$r_{12} = \iiint_{v_1} \iiint_{v_2} f_1(\boldsymbol{v_1}) \sigma(|\boldsymbol{v_1} - \boldsymbol{v_2}|) f_2(\boldsymbol{v_2}) \, |\boldsymbol{v_1} - \boldsymbol{v_2}| d\boldsymbol{v_1} d\boldsymbol{v_2}, \qquad (26)$$

Where f1 and f2 are the distribution functions in the velocity space and $\sigma(|v1 - v2|)$ is the cross section with the corresponding relative velocity. The most relevant cross section for DD and DT fusion reactions is presented in [5] called the Bosch-Hale cross section, which is also presented as a reactivity plot $\langle \sigma v \rangle$ in Figure 2 in Section 1.1. At fusion relevant temperatures, the cross section is strongly dependent on the temperature or the relative velocity. Due to this reason, the relevant ion temperature data is required for calculation of a realistic neutron

production. Other quantities, which affect the production rate and the total production, are the electron temperature, particle densities (implicitly via distribution functions), plasma geometry (including the shape and the total volume), D-T fraction ($^{n}/_{n_T}$) and the heating scheme.

There is a linear dependence on the individual distribution function or particle density in Equation 26, but explicitly, the dependence of temperature is more significant, which can be seen in Figure 2. Experimentally, it has been proved that, the maximum production can be achieved with the D-T fraction 40/60 JET tokamak [15], but generally, the optimum covers range from 40/60 to 60/40 (and it varies shot by shot) and the fuel fraction was quite difficult to control with than 5-10%. As a heat source this point is not so straightforward, since the production rate does not take into account the energy spectra of the fusion products. In DT reactions, the reaction energy is more than five times larger than in DD reactions, but the neutron interactions with materials and the heat transfer efficiency are different. For this reason, many kinds of sensitivity tests are required to optimise of reactor relevant plasma scenarios.

Although, the major part of neutrons is produced in thermal particle reactions in reactor relevant devices, scenario development and validation have to be done in current tokamaks. For this reason, neutrons from thermal-fast reactions are the most significant contribution in validation of all neutron related calculation methods: diagnostics calibration, neutron source routine and nuclear safety analysis.

3.1.2 Fusion alphas

Fusion alphas, and charged fusion products generally, have an important role in plasma control and self-heating. Additionally, they affect strongly the plasma pressure and equilibrium: the additional and significantly large contribution to the total pressure causes the shifting of flux surfaces [13]. This effect has to be taken into account in the scenario modelling, heating and current drive alignment and the control of instabilities.

In ITER size devices, the alpha induced pressure component is estimated to be approximately 30% of the total pressure. This affects significantly the magnetic equilibrium and the repetition of the flux surfaces. In control or measuring of the plasma parameters, especially the current alignment and heating, a well-defined structure of the flux surfaces is needed, consequently ignoring the increased total pressure due to alpha particles can lead to a failure in operation.

Alpha particles are also taking part in many important reactions, of which the most important is the gamma production with beryllium:

$$^{9}\mathrm{Be} + \alpha \rightarrow \mathrm{n} + \gamma + {}^{12}\mathrm{C}.$$

This reaction is significant especially with high energy particles when the initial energy is higher than 1.9 MeV [69]. For this reason, alpha distributions are an input for other synthetic diagnostics: impurity concentration and gamma cameras. This topic is raised in Section 5, when new possibilities of fusion product codes are discussed.

3.2 AFSI ASCOT Fusion Source Integrator

AFSI ASCOT Fusion Source Integrator is a modular code, which defines product distributions in 4D grid (R, z, $v_{\parallel}, v_{\perp}$) based on the given input distributions of reactants in DD, DT and DHe3 fusion reactions (in Publication 3). In the modelling grid, the 3D (x, y, z) velocity has been reduced to the parallel and perpendicular components with respect to the magnetic field vector. AFSI consists of three methods: analytical, semi-analytical and Monte Carlo for solving the production rate integral (presented in Equation 26).

AFSI has been applied as a neutron source for neutron transport calculations in activation and dose rate analysis and also as a synthetic neutron and alpha diagnostics in the JET tokamak (in Publication 3). The unique feature is that also fast particle reactions and spectra can be defined by the AFSI Monte Carlo module. The development of the AFSI Monte Carlo module was driven by a need for a synthetic neutron spectrometer which takes into account also the broadening of the spectrum due to energetic reactive particles. This work was described with more details in Publication 3.

In the Monte Carlo model, the fusion product distribution is calculated by numerically integrating equation 26. It has been implemented by sampling pairs of reactant particles (1 and 2) and collecting the product distributions. Fusion product velocities in 3D are solved from energy and momentum conservation laws in the CM (Center of Mass) coordinates. In the case of DT reactions (neutrons and alphas as the fusion products), momentum and energy conservation can be written as a form

$$m_1\vec{v}_{1,CM}+m_2\vec{v}_{2,CM} = m_n\vec{v}_{n,CM}+m_\alpha\vec{v}_{\alpha,CM} \quad (27)$$

$$E_n + E_\alpha = E_0 = \frac{1}{2}m_1\left|\vec{v}_{1,CM}\right|^2 + \frac{1}{2}m_2\left|\vec{v}_{2,CM}\right|^2 + Q, \quad (28)$$

where Q is the reaction energy and E_0 the total energy defined in the initial state. The fraction of CM velocities $v_{n,CM}/v_{\alpha,CM}$ can be solved from the energy conservation. Direction of the generated neutron can be assumed to be isotropically distributed in the CM sphere coordinates, so based on that the neutron velocity is known and the alpha velocity is solved from the momentum conservation.

In the thermal module, Maxwellian distributions for both reactants are assumed. In this case, the reaction rate is

$$R_{Th} = n_i n_j \langle\sigma v\rangle, \quad (30)$$

where it is calculated analytically, so the distribution functions of products are not available as a result and the spectra have a simple Maxwellian form.

The fast-thermal module is a combination of the functionality of the thermal and fast modules. A Maxwellian distribution is assumed for the thermal reactants, while the fast reactants are given in an arbitrary 4D distribution. Now, the reaction rate is

$$R_{Th-Fast} = \iiint_{v_F}\langle\sigma v\rangle f_F dv_F, \quad (31)$$

where the averaged thermal-fast cross section is

$$\langle \sigma v \rangle = \frac{\sqrt{m_T}}{v_F \sqrt{2\pi}} \iiint_0^\infty \sigma(u) u^2 \left[e^{-m_T (u+v_F)^2 / 2T} - e^{-m_T (u-v_F)^2 / 2T} \right] du \qquad (32)$$

where σ is the differential cross section, v_F is the velocity of fast particles and T is the plasma temperature.

As mentioned, in the semi-analytical and Monte Carlo (for fast particle reactions) modules, distribution functions of reactants are required as inputs. AFSI is implemented to work with ASCOT, when the inputs are coming from the internal calculation loop. On the other hand, any given distribution function can be applied. This makes AFSI benchmarking and validation more fluent. If the thermal or fast-thermal modules are used, the information of the plasma 1D profiles is needed. The interaction between the modules is presented in Figure 16.

The Monte Carlo model is useful especially in diagnostics validation when the spectrum and velocity distribution of the diagnosed particle type is needed. In turn, thermal and fast-thermal modules can calculate production rates quite fast for the inputs for the integrated code systems. For this reason AFSI is coupled to ASCOT in the JINTRAC system and also a connection to the ETS (European Transport Solver) [70] system is under development.

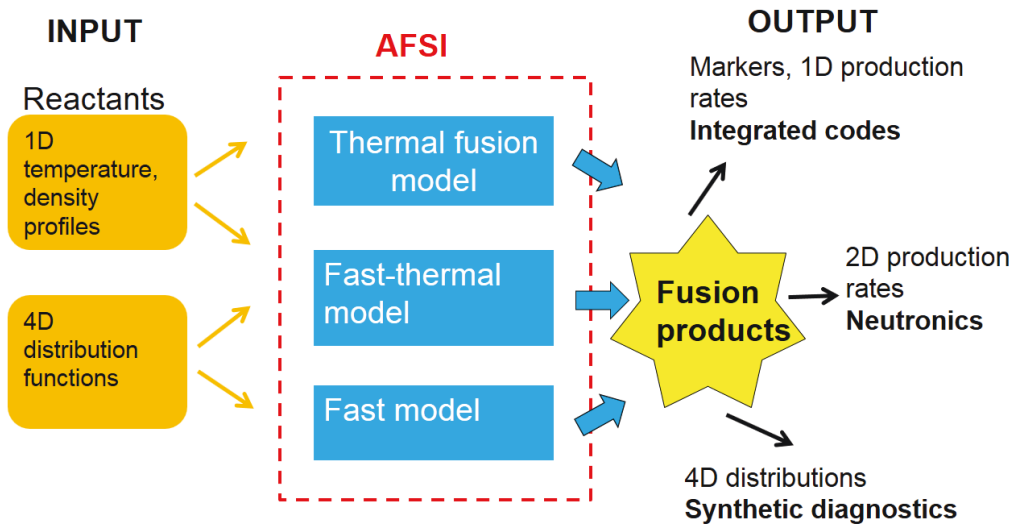

Figure 16. Interaction between the AFSI modules, inputs and outputs (Publication 2).

AFSI fusion production rates have been tentatively validated in JET high performance plasmas with the experimental neutron production rates given by fission chamber diagnostics (KN1) (Publication 2). The validation is presented in Figure 18 where AFSI neutron produc-

tion in different reaction types is presented (with different colour blocks) with the experimental total production. In this official validation plot, data from recent DD plasma experiments were used as input. Differences between measured and calculated production rates are smaller than 20% over the whole time range which was selected for the analysis. Additionally, the sensitivity tests with 10% error bars in the ion temperature profile by AFSI-ASCOT simulations were performed. The difference between measured and calculated neutron rates is smaller than the differences between sensitivity test simulations with the exception of the first data point, where the calculated neutron rate is 2-5% smaller. Additionally, the effect of neutron deficit should be taken into account. High performance plasmas can be used as a validation due to the observed small neutron deficit which is discussed in the chapter 4.2.

The most significant contribution to the neutron rate was achieved by NBI-thermal particle reactions, as assumed. Additionally, the contribution from thermal particle reactions was sufficiently large, 30-60% of the total, in the selected discharge due to the high ion temperature. Fast particle reactions produced approximately 1-2% of the neutrons which is a smaller amount than the contribution from ICRH-thermal particle reactions which were not taken into account in the simulation. Anisotropy in thermal-fast and fast particle reactions can be seen in the 2D production rate maps in Figure 19: fast particle reactions take place closer to the plasma boundary. However, this study was focused on the model validation with the total production rate and the effect of the neutron energy spectrum on the materials or components were not analysed.

As mentioned earlier in Section 3.1.1, the most significant error source is the uncertainty in the ion temperature measurements. The JET discharge #92436 was selected as the validation case, because good quality ion temperature data was available. The ion temperature is measured by charge exchange recombination spectroscopy (CXRS) in fusion applications [67]. In JET, the coverage of the CXRS diagnostics system causes large uncertainty to all analysis: there are no measurement points automatically available in the core plasma inside the half radius.

The other significant point is that the small variations in the solution of the Grad-Shafranov equation cause a shift in the plasma surfaces which changes the differential volume. This leads to different neutron production at the magnetic surfaces which is demonstrated in Figure 17 where integrated neutron production calculated by AFSI with two different plasma shapes from ITER scenarios is presented. In both cases the same 1.5D plasma profiles were used but the mapping to 2D is different due to a different solution of the Grad-Shafranov equation. The integrated plasma volume is 20% larger and neutron production rate almost 30% larger at the half radius when the steady state plasma equilibrium was used. Additionally, plasma pressure, which is not directly measured, is calculated as a sum of the ion and electron pressure including possible errors, such as ion temperature and the lack of the information of fast particle pressure.

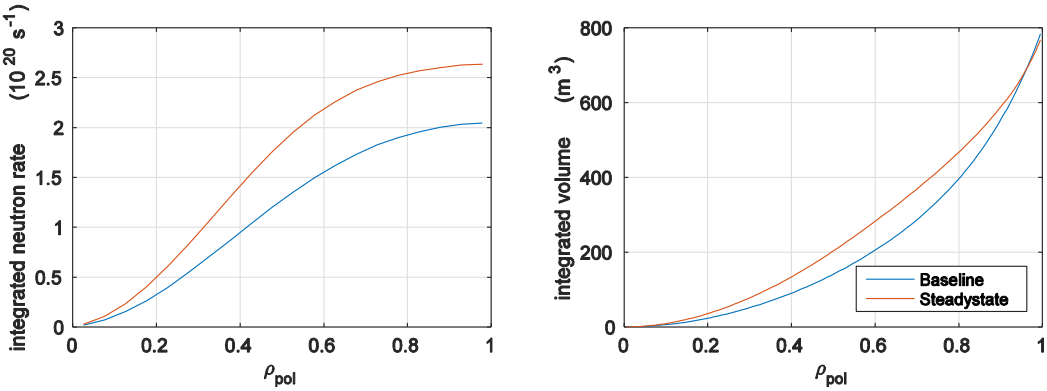

Figure 17. Integrated neutron production rate plasma volume in ITER baseline and steady state magnetic configuration.

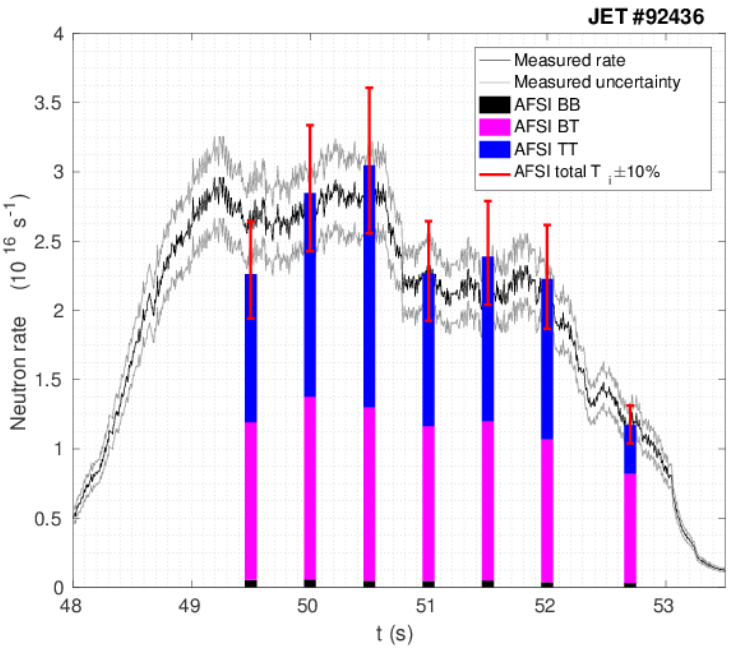

Figure 18. Neutron production rate calculated by AFSI in different reaction types compared with the experimental KN1 values in JET #92436 discharge (Publication 3).

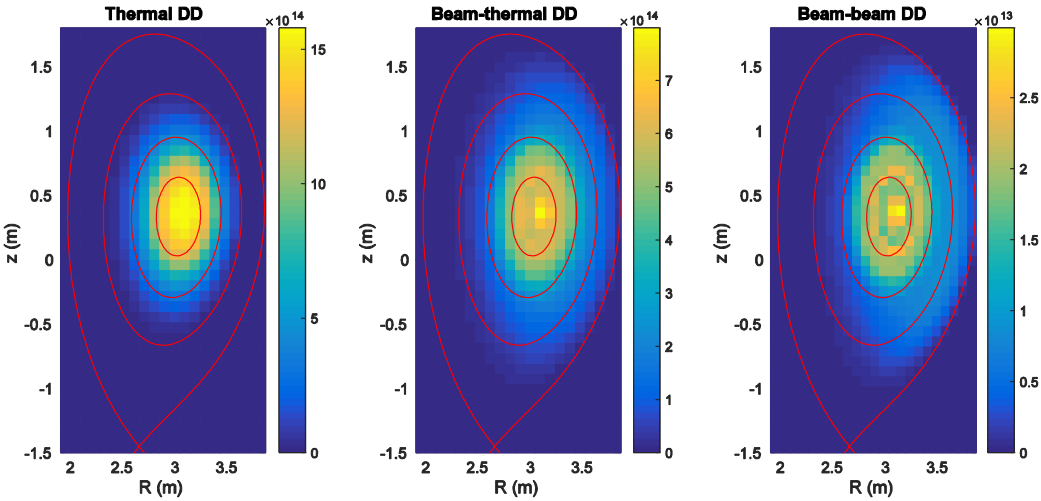

Figure 19. Neutron production rate for different reactions (a) thermal b) fast-thermal c) fast particle) in JET DD plasma calculated by AFSI.

4. Synthetic diagnostics

The main purpose of synthetic diagnostics is to interpret measured data and filter out non-physical effects. They are also generally used in the calibration of real systems, scenario development and the analysis of experiments when the measured data is not available. Additionally, in the case of neutrons, predicted production rates are important also in preparing the experiments, since the fixed neutron budget cannot be exceeded due to safety limits set by the nuclear safety authority.

4.1 The role of neutrons

In forthcoming reactors, 80% of the produced heat will be transferred out from the plasma by neutrons. In contrast, in current experimental devices, neutrons indicate the achieved fusion power. Additionally, due to safety aspects, the total neutron production has to be monitored during the plasma operation. For example, the neutron budget in the forthcoming JET DT plasma campaign (DTE2) is fixed to 1.7×10^{21} neutrons [17]. Material effects, such as radiation damage, are also induced by neutrons. Neutron damage should be estimated for planning shut downs and smaller maintenance work, such as replacing components and diagnostics calibration. In ITER and other reactor relevant tokamaks, changing of components will be done by remote handling manipulators due to the high activation level in the torus. During DT operation, the torus hall and surroundings have to be closed until the activation level has been decreased to acceptable levels.

4.2 Neutrons in JET tokamak

There are several neutron diagnostics systems in operation in JET. Most of them are used to measure the production rate: Fission chambers (KN1) [72, 73] based on the fission reaction in U-235 and U-238 measure the total production continuously. Moveable remotely handled activation sample (KN2) [74] is mainly used in calibration. High spatial resolution neutron camera with 10 horizontal and 9 vertical lines of sight (KN3) [75] covers the whole plasma cross section. It gives the production rate map on the poloidal cross section and is also suitable for gamma measurements. Additionally, two spectrometers are available: Time of flight spectrometer (TOFOR KM11) [76] is measuring the spectrum in one vertical line of sight which is located quite in the centre of the core plasma and the Compact Neutron Spectrometer with a horizontal line of sight [77]. Only fission chamber measurements are operating automatically producing processed data which is generally available in public database and they are required to be switched on as protection diagnostics. Other diagnostics are operated by the experts during plasma discharges but they are usually used only in the experiments where an atypical spectrum is expected.

Generally, large differences between measured and calculated neutron production rates are observed in JET. By comparing mostly used codes, such as TRANSP-NUBEAM [78, 79], neutron production is on average overestimated by 0-100%, which is also presented in Figure 20 [80]. The overestimation varies case by case: typically there is the smallest difference in the plasmas with higher neutron production but any unambiguous reason for the overestimation was not found. This effect is called the neutron deficit [80] and it is one of the most important topics to be studied before the next DT and tritium campaigns, for example due to the limited neutron budget. [18]

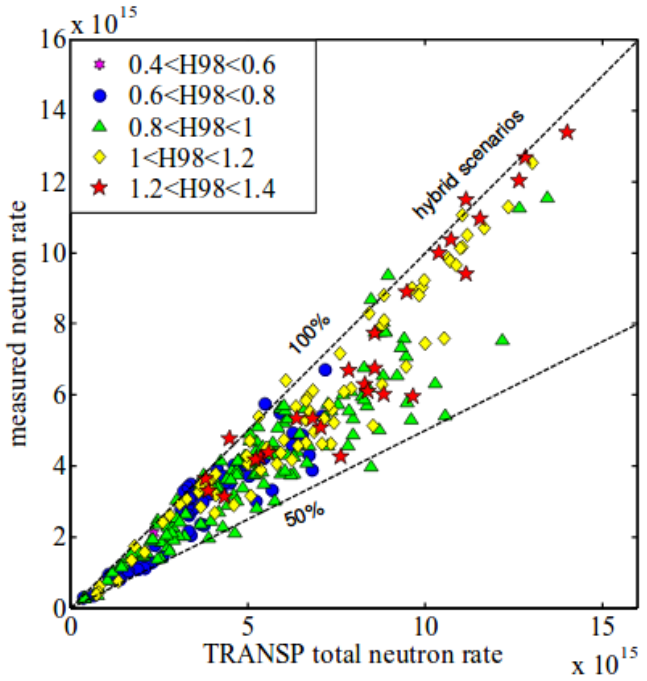

Figure 20. Measured (KN1) vs calculated (TRANSP-NUBEAM) neutron rate in selected JET discharges with ILW [72].

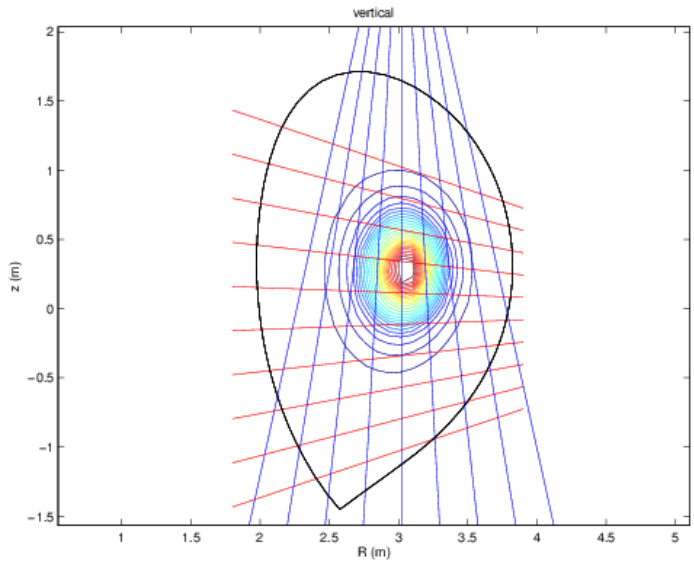

Figure 21. Vertical and horizontal lines of sight in JET KN3 neutron camera.

Synthetic diagnostics are used not only in interpretation of the measurements of physical diagnostics systems but also in the scenario extrapolation. For example, replacing the deuterium beam injector with a tritium one changes the reaction rate and spectra of products due to the different reaction and density of reactants. For this reason, synthetic diagnostics are coupled with the integrated code systems. Especially in reactors, alpha particles (production rate and distribution function) give rise to a significant source term in the heat transport and they contribute to the total pressure.

In the case of synthetic diagnostics in JET, the ion temperature measurements set the limit for the accuracy in the estimated neutron production rate. Typically, the estimated errors in the T_i profile are 10-15% [63]. The neutron production rate can be measured with good accuracy by the fission chambers: errors should be smaller than 8% [73]. So, the ion temperature data can be corrected with the help of predictive simulation which try to match the synthetic neutron production with the experimental one. If good-quality temperature is assumed, the same method can be applied in correcting ion density data correspondingly. On the other hand, the inaccuracy of the measurements of Z_{eff} or identification of impurity species can increase the total error level in the estimated neutron rates. However, these errors are typically lower than in CX diagnostics.

AFSI-ASCOT simulations are used as a basis of the JET synthetic neutron spectrometer, which has geometrical set-up equal to the KN3 neutron camera, which is presented in Figure 21. This synthetic AFSI-based diagnostics was implemented as an ideal diagnostics without detector related effects, scattering or attenuation for instance. However, AFSI is implemented as a part of the calculation chain including also neutron transport calculated by Serpent. In the near future, this chain will be supplemented with tools for more realistic detector modelling.

The need for a simple-to-use tool to define fast-thermal and fast particle reaction-based neutron production rates and spectra for DT extrapolation and neutron deficit studies was the main motivation to implement AFSI-ASCOT based synthetic neutron diagnostics. AFSI has also many other benefits. It is quite fast, because the Monte Carlo module is only used on fast particle reactions and any given distribution function (in fixed format) can be used. That makes benchmarking and sensitivity tests straightforward. It is coupled to the integrated code package such as JINTRAC and ETS, so it is suitable to use in scenario modelling and the inputs are easy to generate. The AFSI-based neutron source is also the part of calculation chain where the plasma physics, neutron transport in the material and thermo-hydraulic analysis are coupled. This calculation chain is remarkable because, traditionally plasma physics and neutronics as a part of reactor analysis have been quite separate fields. Generally, very rough parametrised models of the neutron source [81] are used in neutronics. Instead, the detailed AFSI-based model enables study of plasma related effects, such as wider spectrum and source geometry in neutron transport.

One of the most analysed DD record shots (#86614) was selected for the validation of synthetic KN3. Qualitative results from the KN3 camera were available and the calculated production rates have been compared with those ones. The scaled experimental production rates have been presented with AFSI results (see also Figure 22) in Figure 24. Additionally, the spectrum in the extreme case with high energy reactants generated by ICRF third harmonic heating [82] has been compared with the spectrum calculated by alternative synthetic diagnostics based on the ControlRoom code [65].

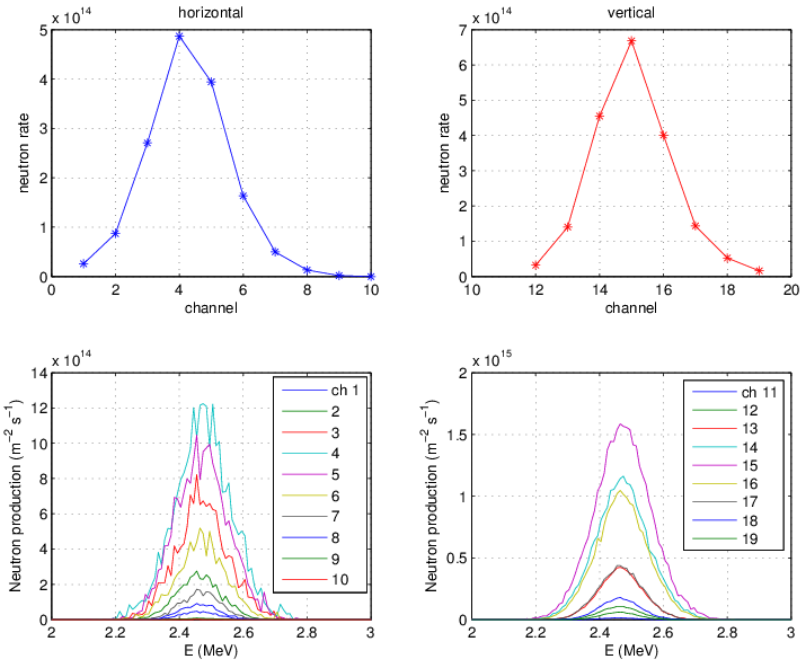

Figure 22. Production rates (top) and neutron spectra (bottom) in JET #86614 discharge defined by AFSI based synthetic KN3 camera.

Maximum production was observed in the fourth channel horizontally and in the fifteenth channel vertically in the physical KN3 measurements. Also in AFSI-based production rates the maxima are achieved in the same channels and the amount of order is the same for computational and measured values with the exception of the outermost vertical channels 11, 12, 13 and 19. Computational values were overestimated in channels 11, 12 and 13 (the leftmost lines in Figure 21) and the production was underestimated in channel 19. Those differences are probably caused by detector related effects but also errors in the equilibrium reconstruction can affect the total plasma volume and production rate. Similar effects were observed also in [82].

Spectrum calculation was validated with the ICRH heated shot #86459 where the reactant distribution was notably anisotropic. The spectrum covers energies between 1.6-5.4 MeV (peaking at 2.5 and 3.0 MeV energies) which corresponds qualitatively with the spectrum calculated by an alternative tool, ControlRoom [65]. This comparison is presented in Figure 23.

As mentioned, KN3 experimental values are given as counts of detector. The calibration coefficients were not available and defining them is challenging in any case. The most appropriate way to do quantitative validation is by doing neutron transport calculation including the modelling of detector.

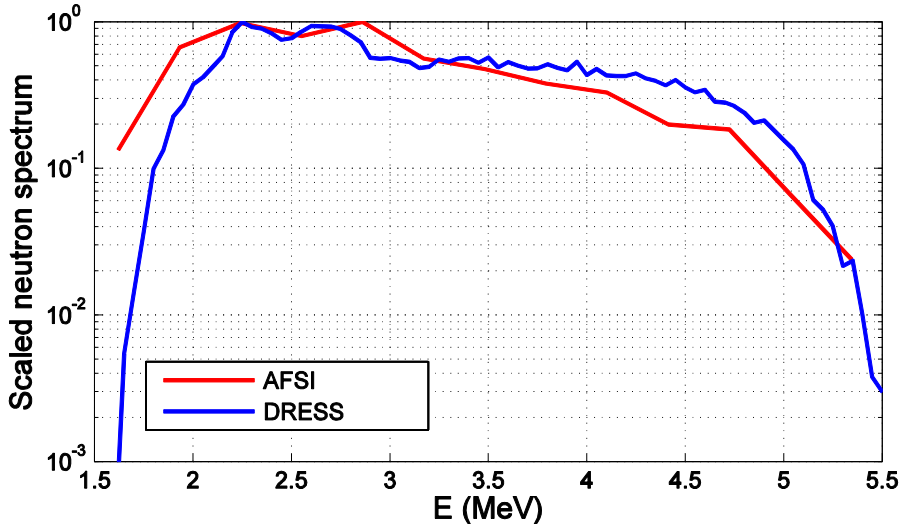

Figure 23. Production rates and neutron spectra in JET #86614 discharge defined by AFSI (red) and ControlRoom (blue) [65] based synthetic TOFOR.

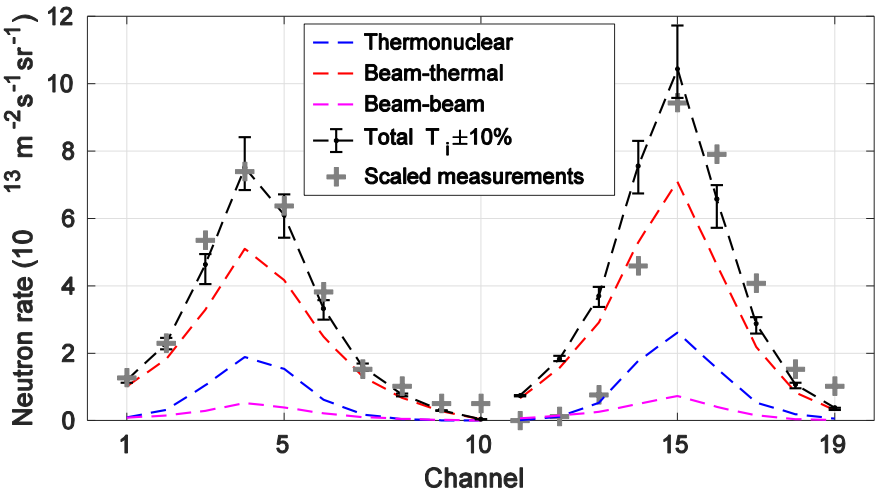

Figure 24. Production rates and neutron spectra in JET #86614 discharge defined by AFSI in different reaction types with error estimates due to 10% variations in T_i compared with KN3 neutron camera scaled measurements.

5. Plasma analysis calculation chain

The development of the calculation chain ASCOT-AFSI-SERPENT-APROS started in 2014 with the aim of DEMO balance-of-plant analysis. After three years, the use of different modules has been demonstrated with real fusion applications and they are now being used in the analysis of several fusion devices and projects, such as the most important of them, ITER neutronics and JET synthetic diagnostics.

The above mentioned calculation chain includes the following coupled tools described from the fuel plasma to the power plant secondary loop

- ASCOT [52-53]
  Defining the distribution function of reactive plasma particles
- AFSI [Publication 2]
  Generating the neutron production and spectra to the Serpent input
- SERPENT [83]
  Calculating the neutron and gamma transport to evaluate the parametrised heat source coupled to the power plant component models
- APROS [84]
  Modelling the power plant processes

The unique feature in the calculation chain is the detailed description of the plasma neutron source based on the interactions between the fuel particles via ASCOT. ASCOT can be also coupled to scenario modelling code systems, which enables fully predictive modelling and systematic handling of input data. Due to this connection, all effects of the neutron production can be analysed efficiently by sensitivity tests. The tools for the calculation chain are mainly developed at VTT in close collaboration with Aalto University and also internationally at JET (ASCOT and AFSI), which decreases the possible lack of information and feedback from the users and experts.

5.1 Serpent neutron source

The Serpent Monte Carlo code has been developed for reactor physics calculations at VTT since 2004, with the main purpose of producing spatially homogenised group constants for deterministic fuel cycle and transient simulator codes [83]. In recent years the built-in capabilities in Serpent have been extended to cover a broader scope of reactor physics applications, in particular multi-physics simulations involving the internal and external coupling of Monte Carlo neutronics to fuel performance and thermal hydraulics.

The development of new applications of Serpent to different fields including fusion neutron and gamma transport, radiation shielding and medical applications started actively in 2015. Recently developed features, the photon transport mode and CAD-based geometry model, have been key drivers in extending Serpent into applications in these new fields.

Compared to fission reactors, a more detailed geometrical description is needed in fusion applications. Additionally, the range of materials and isotopes is wider and more different reactions, such as threshold reactions due to higher energies of particles, have to be included to the modelling scope. The principle of Serpent neutron source block is presented in Figure 25. The source routine generates Monte Carlo based source neutron distribution based on the pre-calculated probability distributions on three levels:

- Probability of the reaction type (thermal DD/DT, fast-thermal DD/DT, fast DD/DT)
- Probability of position (in Rz or rho-theta grid)
- Probability of energy/direction or velocity

First, the reaction type (DD or DT and the energy range fixed: thermal, fast-thermal, fast) is sampled from the probability distribution which is formed based on the fraction of production rate for each reaction. On the next level, the location on the poloidal cross section (2D or 1.5D information can be used) is defined on the same geometry grid for every reaction type: index in (R, z) pair or ρ distribution is sampled based on the reaction rate profile. The source routine includes the information of energy spectra or velocity components for every grid point. On the third level, the energy and pitch or velocity components are sampled. Neutrons can be generated and the source probability distributions calculated separately for every reaction type. In addition, the source routine includes the total production per reaction type for the normalisation.

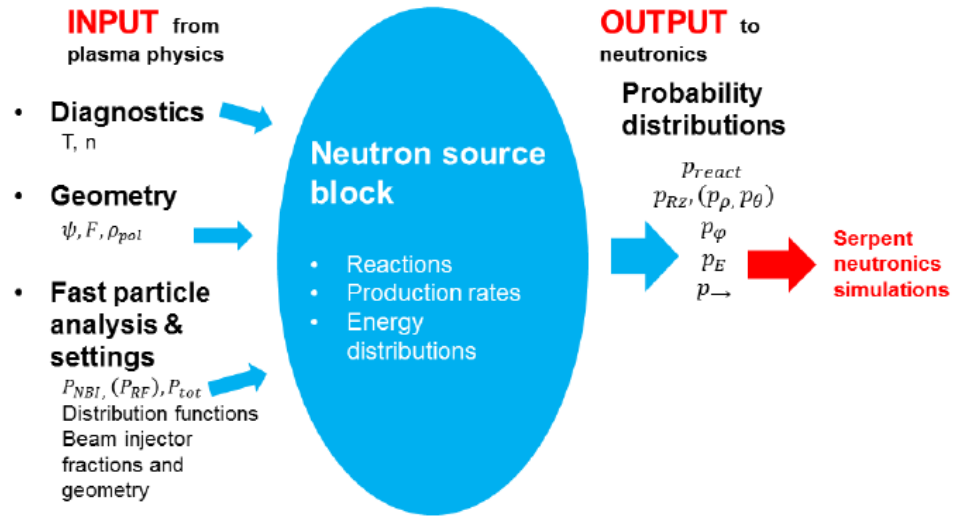

Figure 25. Neutron source and its inputs and outputs in the Serpent code (Publication 4)

5.2 Applications

As mentioned, the calculation chain has been tested module by module in different applications. In current devices, such as JET, the main application presently is in the field of synthetic diagnostics whereas in forthcoming devices, like ITER, the focus is to the operation design within the safety limits. The synthetic neutron diagnostics in JET was implemented by AFSI-ASCOT in 2016 and it is briefly reported in Section 4.2

All modules in the calculation chain are combined in the balance-of-plant analysis. Completed analysis requires also new added features, such as modelling and parametrisation of radiated heat and divertor heat loads. However, the tools for various modelling purposes are available in the existing version of the calculation chain. ITER is probably the largest field of applications: heat deposition, tritium breeding and material damage are essential topics where the AFSI-SERPENT part of the chain can be utilised.

5.2.1 Serpent fusion neutron and gamma transport: case ITER

Serpent capabilities in fusion applications have been presented in the reference papers in [Publication 4, 85], which is the first fusion related Serpent work reference. The ITER baseline and steady state scenarios with the energy multiplication Q = 10 and Q = 5, respectively, and D/T mix of 50%/50% (the parameters which were used are listed in Publication 4) were selected to the demonstration case. The neutron production rates are given in rho-theta coordinates by AFSI coupled to the JINTRAC due to faster calculation time and easy handling of inputs and outputs.

The AFSI-SERPENT coupling has to be validated before large-scale applications. The most of this work has been done in JET where good neutron diagnostics and valid experimental data are available. AFSI modules (analytical, semi-analytical and Monte Carlo), have been benchmarked against other codes in extreme cases (total production, thermal and ICRH based high energy neutrons), as presented in the Publication 3.

The total neutron production rates (from thermal and fast-thermal reactions) given by AFSI, the 2D source geometry and cumulative probability distributions are used to generate the Serpent neutron source. The source, which is plotted in Figure 26, shows that in the steady-state scenario the total neutron rate is lower, and additionally the rate profile is more peaked to the outer radius. This causes the maximum source neutron distribution to be further from the magnetic axis than in the baseline case. Another significant difference is the poloidal shape of source and mapping of flux surfaces which spans the production rates to the grid. Those effects appear to be rather small, but they can cause large differences in the total neutron production.

As mentioned, the major part of neutrons is produced in the thermal particle DT reactions in ITER. However, the other reactions have to be taken into account in validation and additionally in the analysis of the non-nuclear phase. A significant issue is also the damage of sensitive components, such as diagnostics, due to high energy neutrons. Spatial neutron distribution in different reactions types for DD reaction is presented in Figure 27. These reaction rate maps show that the neutron production is strongly localised, especially in fast-thermal and

fast particle reactions, which can cause different high energy neutron fluxes with different poloidal angles.

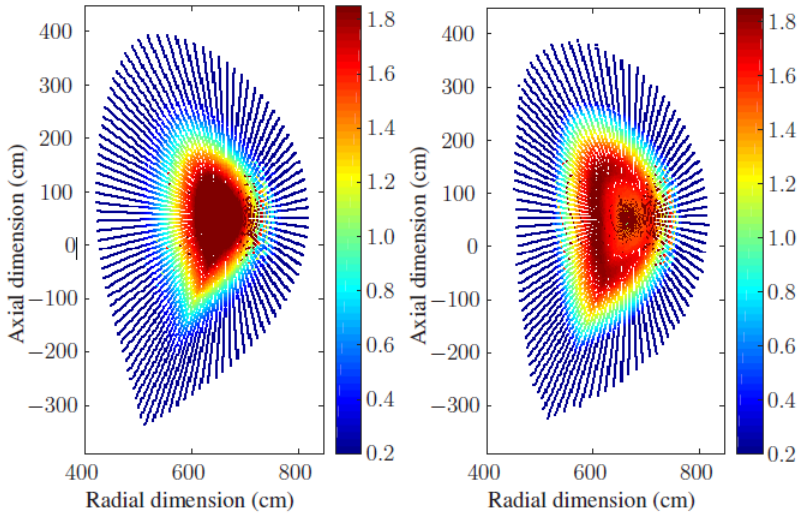

Figure 26. Serpent neutron source distribution in ITER DT plasma baseline (left) and steady state (right) scenarios in arbitrary units.

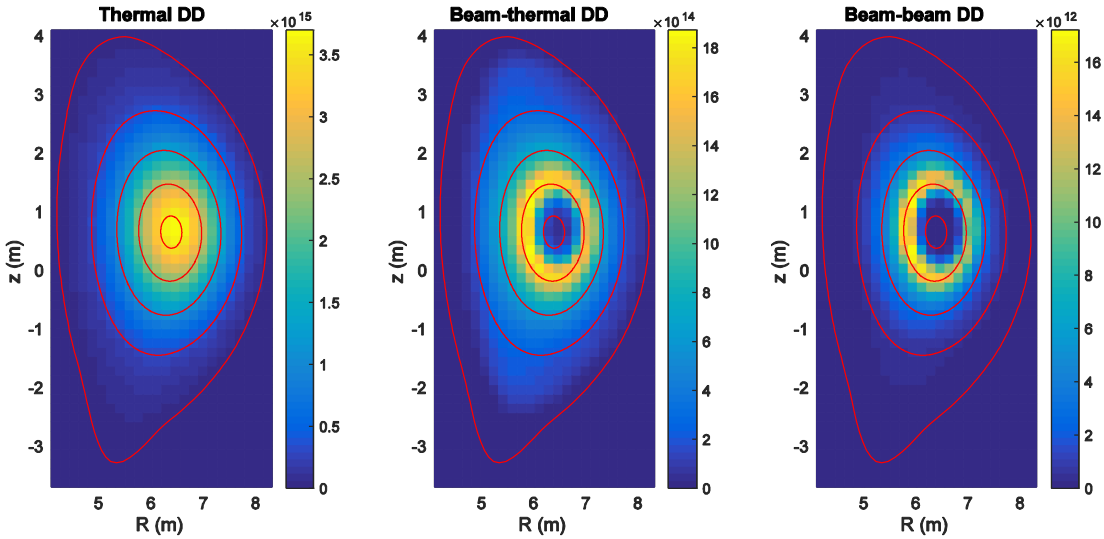

Figure 27. Neutron production rate for different reactions (a) thermal b) fast-thermal c) fast particle) in ITER DD plasma baseline scenario.

5.2.2 Balance-of-plant analysis

Balance-of-plant consists of the dynamic process modelling of power plant subsystems and parametrised volumetric heating calculated by coupled neutron and gamma transport and neutron production in the fuel and the interface with the integrated modelling tools is presented in Figure 28. Until recently, the modelling of power plant processes in fusion applications has been strongly separated from the physical effect in the plasma fuel. However, rough parametrisation of the plasma profiles does not take into account all effects, such as strongly localised neutron production, which can cause reactions in the materials and changes in heat production.

A broad expertise of different fields is required in the balance-of-plant modelling. Due to this reason, one of the most important features in the coupled system is an easy-to-use options and smooth interaction between the modules. Additionally, using the same tools in different applications improves their quality when the same method is validated by several users.

Key questions in the balance-of-plant analysis are for instance:

- Maximising the heat transfer to the secondary loop
- Operation with the heat storage system between the plasma pulses
- Optimisation of the blanket cooling
- Tritium breeding.

Particularly, there is a need for a detailed description of the energy production in the plasma and the energy transfer via neutrons in all these goals. Particularly, tritium breeding will be one of the most significant tasks in ITER studies and the efficiency of the breeding depends on the energy spectra of neutrons which induce the reaction in lithium and in potential neutron multiplier materials, such as lead.

As mentioned in the beginning of Section 5, coupling of the tools in plasma physics and power plant processes makes the modelling work more fluent, for example due to the systematic handling of the inputs and outputs. Additionally, the reason for the behaviour is easier to observe, when the whole chain of analysis is available and well-known.

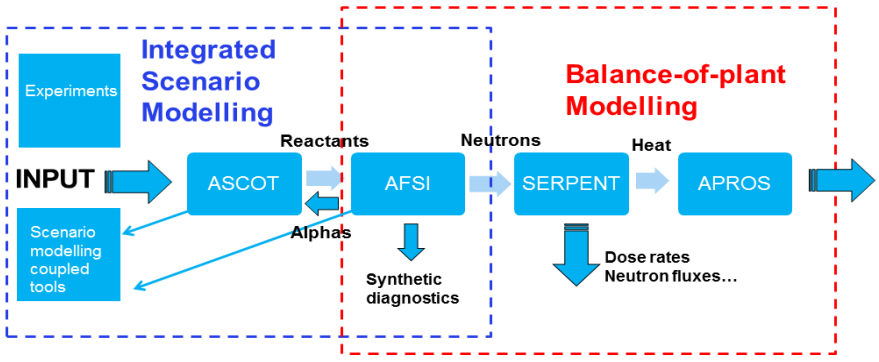

Figure 28. Interaction between scenario modelling and balance-of-plant modules

6. Conclusions

Reactor relevant plasmas are studied to maximise energy production and the efficiency of power plant operation. There are technical challenges as well as requirements related to long pulse length and plasma control to be taken into account in the scenario development for future devices but also for today's experiments. This connection between plasma physics and technology will be essential and the interaction of these – yet somewhat separate – fields will increase in forthcoming years towards ITER and DEMO. In this thesis, plasma related effects that can affect technical solutions, such as heat production, pulse length and material activation have been studied.

The properties of reactor relevant plasmas and the coupling of plasma physical effects and neutronics are studied using different views in this thesis. Publication 1 focuses on advanced tokamak scenario plasmas. The basis was the analysis and extrapolation of the identity plasma experiments in two large tokamak devices in JET and JT-60U with matching plasma parameters. During the experiments, these tokamaks were the most relevant and largest devices for ITER studies. However, these same-size devices were fundamentally different due to heating capabilities and the shape of the plasma. Different behaviour of plasma density and current has been studied by predictive current diffusion simulations with the JINTRAC coupled code system. The most significant and previously not analysed results are related to the role of geometry in achieving steady-state and the production of the bootstrap current. Changes of the geometrical parameters seem to be the most promising way to achieve a steady-state in JET. The connection between the bootstrap fraction, geometry and obtained density gradient was observed and deduced to be one of the most significant differences between JET and JT-60U.

Publication 2 is the reference paper to AFSI which is a new fusion product module of the ASCOT particle following code. Fusion products, mainly helium and neutrons, can be characterised with a production rate and spectrum by AFSI where all relevant fusion reactions (DD, DT) with all energies of reactants can be calculated. The most important reason to implement the new module was to use it as a part of calculation chains in different fields of applications: neutronics, alpha particle physics, synthetic diagnostics and calibration of diagnostics systems for instance. Additionally, one beneficial feature is that AFSI is very versatile and extensible for different reaction types, TT fusion and gamma production, for example. This gives more new possibilities for further development.

Publication 3 reports on a direct application of AFSI: synthetic neutron camera and spectrometer in JET. This synthetic neutron and alpha diagnostics system which replicates the geometry of the real neutron and gamma camera in JET can be also expanded to gamma

production. Tentative validation of AFSI has been performed with data from extreme cases in JET plasmas and good level of agreement was achieved regarding that the most significant uncertainty in the results comes via the effect of the ion temperature on the cross sections.

Publication 4 describes the neutron transport calculation procedure with the Serpent code in fusion applications and especially, generating the plasma neutron source. Fusion neutron source was a completely new feature in Serpent and the fusion applications give many new, not only scientific but also business related development possibilities for it. The whole calculation chain from plasma physics in the fuel to thermo-hydraulics in the cooling of blanket is needed in ITER and particularly in designing DEMO.

The calculation chain, especially the coupling of Serpent, ASCOT and AFSI development is mainly performed in a Finnish collaboration between VTT and Aalto University. For this reason, further development is efficient and rather expeditious without any delays due to information delivery and different work flows. However, the international collaboration has been an essential part of the work from the beginning and there is quite a large user community for each code. ASCOT has been used in the analysis of many tokamak devices for years and it has an established position in European fusion research, so AFSI will be taken to use as a natural extension. Also Serpent is widely used in the fission community where its methods and procedures have been tested and validated. As mentioned, the strongest features are the detailed description of fusion neutron source and the capability to expand it to calculation chains in fusion applications in tokamaks but in stellarators as well.

References

[1] World Resource Institute, CAIT Climate Data Explorer, cait.wri.org, cited 3/2017
[2] International Energy Agency. 2016. World Energy Outlook 2016, OECD/IEA
[3] International Energy Agency. 2016. Energy and Air Pollution, OECD/IEA
[4] International Energy Agency. 2016. CO2 Emissions from Fuel Combustion, IEA
[5] Bosch H. S., Hale G. 1992. Nucl. Fusion 32 611
[6] U-235, U-238 fission cross section data: ENDF/B-VIII.b4, IAEA Consortium
[7] Lawson J. D. 1957. Proceedings of the Physical Society B 70 6
[8] Tamm I. E., Sakharov A. D. (ed. by M. A. Leontovich). 1961. Pergamon Press Vol 1
[9] Wesson J. 2004. *Tokamaks*. 3rd edition. Oxford University Press
[10] Cordey J. G. et al. 1988. Plasma Phys. Control. Fusion 30 11 1625-1635
[11] Fisch N. J. 1987. Rev. Mod. Phys. 59 175
[12] Kruskal M. D., Kulsrud R. M. 1958. The Physics of Fluids 1958 1 265-274
[13] Shafranov V. D. 1958. Soviet Journal of Experimental and Theoretical Physics 6 545
[14] Rebut B. H. et al. 1985. Nucl. Fusion 25 1011
[15] Rebut P. H. 1992. Plasma Phys. Control. Fusion 34 1749.
[16] Keilhacker M. et al. 1999. Nucl. Fusion 39 209
[17] Weisen H. et al. 2014. AIP Conference Proceedings 1612 77
[18] ITER Physics Basis (updated). Overview and Summary. 2007. Nucl. Fusion 47 S1—S17
[19] Matthews G. F. 2011. Physica Scripta T145 014001
[20] Romanelli F. et al. 2015. Overview of the JET results. Nucl. Fusion 55 104001
[21] Wenninger R. et al. 2015. Nucl. Fusion 55 063003
[22] Wiesen S. et al. 2008. JINTRAC-JET modelling suite. JET ITC-Report
[23] Romanelli M. et al. 2014. Plasma and Fusion Research 9 Special Issue 2
[24] Genacchi G., Taroni A. 1988. “A free-boundary plasma transport code”. JET-IR(88)03
[25] Lauro-Taroni L. et al. 1994. Proc. 21st EPS I 102
[26] Reiter D. 1992. J. Nucl. Mater., 196-198, 80-89
[27] Simonini, R. et al. 1994. Contrib. Plasma Phys. 34 368
[28] Luce T. C. et al. 2008. Plasma Phys. Control. Fusion 50 043001
[29] Petty C. C. 2008. Phys. Plasmas 15
[30] Engelmann F. 1990. Plasma Phys. Control. Fusion 32 1101
[31] Taylor T. S. et al. 1997. Plasma Phys. Control. Fusion 39 B47
[32] Green B. J. et al. 2003. Plasma Phys. Control. Fusion 45 687
[33] Luce T. C. et al. 2014. Nucl. Fusion 54 013015
[34] Kikuchi M. et al. Plasma Phys. Control. Fusion 35 Supplement B
[35] Houlberg W. A. et al. 2005. Nucl. Fusion 45 1309-1320
[36] Wagner F. et al. 1982. Phys. Rev. Lett. 49 1408
[37] Koide Y. et al. 1994. Phys. Rev. Lett. 72 3662
[38] Gormezano C., A. Fasoli A. 1996. Proc. 16th IAEA International Conference on Fusion Energy, Montreal, Canada, October 1996
[39] Sakamoto Y. et al. 2009. Nucl. Fusion 49 9

[40] Joffrin E. 2007. Plasma Phys. Control. Fusion 49 B629
[41] Garcia J., Giruzzi G. 2012. Plasma Phys. Control. Fusion 54 015009
[42] de Vries P. C. et al. 2009. Plasma Phys. Control. Fusion 51 124050
[43] Litaudon X. et al. 2011. Nucl. Fusion 51 073020
[44] Koch R. 1998. Transactions of Fusion Tech. 33 2T
[45] Koch R. 2013. Proceedings of the Carolus Magnus Summer School on Plasma and Fusion Energy Physics 2013 274-281
[46] Duesing G. et al. 1987. Fusion Sci.Tech. 11 163-202
[47] Stix T. H. 1975. Nucl. Fusion 15 737
[48] Hinton F. L., Hazeltine R. D. 1976. Rev. Mod. Phys. 48 239
[49] Hirsman S. P., Sigmar P. D. 1981. Nucl. Fusion 21 0179
[50] Stroth U. et al. 1991. Nucl. Fusion 31 2291
[51] Ongena J. P. H. E. et al. 2012. Transactions of Fusion Sci. Technol. 61
[52] Kessel C. E. 1994. Nucl. Fusion 34 1221
[53] Kikuchi M. 1990. Nucl. Fusion 30 265
[54] Peeters A. G. 2000. Plasma Phys. Control. Fusion 42 B231–B242.
[55] Litaudon X. et al. 2006. Plasma Phys. Control. Fusion 48 A1
[56] Heikkinen J. A. et al. 2001. J. Comput. Phys. 173 527-548
[57] Hirvijoki E. et al. 2014. Comput. Phys. Commun. 185 1310-1321
[58] Asunta O. et al. 2015. Comput. Phys. Commun. 188 33-46
[59] Houlberg W. A. 1997. Phys. Plasmas 4 3230
[60] Polevoi A., Kavin A. 2002. ITER plasma data for Scenario 4 (during burn). ITER D 22KZM2 v1.0. https://user.iter.org/?uid=22KZM2
[61] Oyama N. 2009. Nucl. Fusion 49 104007
[62] Sips A. C. C. 2005. Plasma Phys. Control. Fusion 47 A19-A40
[63] Houlberg W. A. et al. 2005. Nucl. Fusion 45 1309-1320
[64] Hoang G. T. 2009. Nucl. Fusion 49 075001 11pp
[65] Ballabio L. 2008. *Control Room 0.3.7 User Manual*
[66] Eriksson J. et al. 2015. Nucl. Fusion 55 123026
[67] Nocente M. et al. PhD Thesis http://hdl.handle.net/10281/28397
[68] Tardocchi M. et al. 2011. Phys. Rev. Letters 107 205002
[69] Kiptily V. et al. 2005. Nucl. Fusion 45 L21
[70] Coster D. et al. 2010. IEEE Trans. Plasma Sci. 38 2085
[71] Giroud C. et al. 2008. Rev. Sci. Instrum. 79 525
[72] Jarvis O. N. et al. 1985. Europhys. Conf. Abstracts Vol. 9F, Part 1, p. 223
[73] Syme D.B. et al. 2012. Nucl. Eng. Des. 246 185-190
[74] R. Prokopowicz et al. 2011. Nucl. Inst. Methods A 637 119-127
[75] Adams J.M. et al. 1993. Nucl. Inst. Methods A 329 277-90
[76] Hjalmarsson A. et al. 2003. Review of Scientific Instruments 74 1750
[77] Belli F. et al. 2012. IEEE Transactions on Nuclear Science 59 2512-2519
[78] Budny R. V. et al. 1994. Nucl. Fusion 34
[79] Pankin A. et al. 2004. Comput. Phys. Commun. 159 157-184
[80] Weisen H. et al. 2017. *The "neutron deficit" in the JET tokamak*. To be submitted to Nucl. Fusion
[81] Fausser C. et al. 2012. Fus. Eng. Des. 87 787-792
[82] Schneider M. et al. Nucl. Fusion 56 112022

[83] Eriksson J. et al. 2015. Nucl. Fusion 55 123026
[84] Leppänen J. et al. 2015. Ann. Nucl. Energy 84 55-62
[85] Official web site *APROS*: www.apros.fi/
[86] Leppänen, J. and Kaltiaisenaho, T. 2016. *Expanding the Use of Serpent 2 to Fusion Applications: Shut-down Dose Rate Calculations.* In proc. PHYSOR 2016, Sun Valley, ID, May 1-6, 2016

Publication 1

P. Sirén, T. Tala, G. Corrigan, J. Garcia,T. Koskela, F. Köchl, X. Litaudon, A. Salmi, JET EFDA contributors and the EU-ITM ITER Scenario Modelling Group. 2015. Understanding of the fundamental differences in JET and JT-60U AT discharges. Plasma Physics and Controlled Fusion 57 075015.

Publication 2

P. Sirén, J. Varje, S. Äkäslompolo, O. Asunta, C. Giroud, T. Kurki-Suonio, H. Weisen. 2018. ASCOT Fusion source integrator AFSI for fast ion and neutron studies in fusion devices. Nuclear Fusion 58 016023.

Publication 3

P. Sirén, J. Varje, H. Weisen, T. Koskela. 2017. Synthetic neutron camera and spectrometer in JET based on AFSI-ASCOT simulations. Journal of Instrumentations 12 C09010.

Publication 4

P. Sirén, J. Leppänen. Expanding the use of Serpent 2 to fusion applications: Development of a neutron source. In proc. PHYSOR 2016, Sun Valley, ID, May 1-6, 2016.

EXPANDING THE USE OF SERPENT 2 TO FUSION APPLICATIONS: DEVELOPMENT OF A PLASMA NEUTRON SOURCE

Paula Sirén and Jaakko Leppänen
VTT Technical Research Centre of Finland, LTD
P.O. Box 1000, FI-02044 VTT, Finland
Paula.Siren@vtt.fi

ABSTRACT

Methodology for fusion neutronics calculations is currently being implemented in the Serpent 2 Monte Carlo code. The work is focused on two main topics: 1) Development of a new source routine used for coupling the output of plasma scenario codes into the neutron transport simulation, and 2) An advanced CAD-based geometry type capable of modeling the complex structures encountered in fusion applications. The new geometry model was demonstrated in a recent study, using the C-Lite CAD model of the ITER fusion reactor as the test case [1].

This paper continues the previous work with the demonstration of the plasma source routine. Two plasma scenarios, corresponding to baseline and steady-state operating modes of the ITER reactor are first modeled using the AFSI and JINTRAC plasma codes, and the resulting source distributions used in Serpent 2 neutron transport simulations. Because of certain deficiencies in the geometry model, the results cannot be considered physically realistic. For this reason the test cases presented here should instead be considered a practical demonstration of the developed calculation sequence.

The work for expanding the use of Serpent into fusion neutronics is still at a relatively early stage. Potential future applications include heat deposition, material damage, tritium breeding and various radiation shielding applications. The neutronics calculations in this study are also used to provide activated material compositions for shut-down photon dose rate calculations, presented in another paper at this conference [2].

Key Words: **Serpent, fusion neutronics, plasma scenario modeling, neutron source, ITER**

1. INTRODUCTION

The Serpent Monte Carlo code has been developed for reactor physics calculations at VTT Technical Research Centre of Finland since 2004, with the main purpose of producing spatially homogenized group constants for deterministic fuel cycle and transient simulator codes [3]. In recent years the built-in capabilities in Serpent have been extended to cover a broader scope of reactor physics applications, in particular multi-physics simulations involving the internal and external coupling of Monte Carlo neutronics to fuel performance, thermal hydraulics and CFD codes [4]. For these traditional and novel

applications Serpent is currently used in 148 universities and research organizations in 37 countries around the world, with the total number of users around 500.

Within the growing user community there has been an increasing interest to broaden the scope of applications even further, beyond fission reactor physics. This goal is supported by recent work on a photon transport simulation mode [5], carried out for the purpose of gamma heating in multi-physics applications, as well as the introduction of advanced unstructured mesh [6] and CAD-based geometry types [1], originally developed as the by-product of a multi-physics interface for CFD code coupling. The potential future applications for Serpent include radiation shielding, medical physics and space applications, but in particular fusion neutronics.

This paper presents the first part of a study, in which the new capabilities of Serpent are demonstrated in fusion applications. The test case is a realistic CAD-based geometry model of the ITER fusion reactor. Two plasma scenarios, a baseline and a steady-state case are simulated using the AFSI and JINTRAC plasma codes and the resulting fusion neutron source distributions coupled to Serpent via the newly-developed source routine. Serpent is used for calculating spatial flux and absorption rate distributions, as well as activation caused by neutron-induced reactions. The activated materials form the source term for the second part of the study, involving shut-down gamma dose rate calculations. The results of the second part are presented in another paper at this PHYSOR 2016 conference [2].

This work is part of a long-term effort to develop a new computational framework for fusion neutronics, combining Monte Carlo particle transport calculation, plasma scenario simulations and CAD based geometry modeling in a highly-integrated way. Providing new high-performance, high-fidelity modeling tools capable of covering the full scope of fusion neutronics analyses is considered valuable to the international fusion neutronics community, facing increasingly complicated engineering challenges as the research is moving towards the design and construction of large-scale experimental and demonstration devices. The work is still at an early stage, and the purpose of this and other preliminary studies is to demonstrate that Serpent is a practical candidate for such analyses.

2. PHYSICAL BACKGROUND

Generally, fusion reactions (DD and DT) in magnetically confined plasmas can be divided in three groups. The majority of the reactions belongs to group (1), thermal particle reactions, which consists of the reactions between thermal or Maxwellian distributed target plasma ions (energy interval 1-40 keV). Group (2), fast particle (energies $>$ 50 keV) reactions, includes the reactions between high energy (or additionally heated) ions produced by neutral beam injections (particle energies in NBIs will be 1 MeV in ITER heating system) or radio frequency wave resonances. Additionally, group (3) is a combination of groups (1) and (2), containing reactions between thermal and fast particles.

Regarding neutron production, thermal reaction group is the most important source which produces the major part of neutrons in the plasma globally in reactor-relevant-sized devices. The fraction between

group (1) and (2) varies globally between 80% and 99.5% in typical high-gain fusion plasmas (such as JET DT record shots and ITER reference plasmas), depending mainly on temperature, total plasma volume and mix of fuel (D, T, impurity accumulation). However, in current devices like JET, the fraction of neutrons produced by fast particle reactions is more significant and it may strongly affect the neutron energy spectra.

The major part of the source, contributed by the neutrons produced by thermal particle reactions, is constant on the poloidal flux surface which is based on the constant temperature at the normalized radial coordinate. Neutrons from reactions in group (2) and (3) have strongly asymmetric distribution on the poloidal cross section due to alignment of the heating systems. Universally, it can be noted that the part of neutrons produced by reactions in group (2) and (3) is minor (see the total fraction of thermal and fast particles) but not negligible, and it can have an important role in local neutron production profile and energy distribution of fusion products. Additionally, the role of spatially anisotropic energy distribution can be significant in the complete neutronics calculations.

However, group (2) is important in test or validation cases with current-size devices, so it will be implemented in the neutron source model for the validation and method testing particularly. The part of fast particle reactions concentrated on the reactions between NBI particles in this paper, but practically, fast particle distribution from any source can be analyzed by changing the velocity distribution of reactive particle source. Heretofore, simplified analytical methods which are based on the conversion of experimental or fitted data profiles to the D-shape plasma geometry approximation have been used as the plasma neutron source to neutronics calculations. Additionally, neutron production in fast particle reactions has usually been ignored in earlier analyses and, overall, anisotropic distributions (in the production rate and energy of the produced neutrons) have not been considered in the earlier neutron source models.

3. GENERATING THE NEUTRON SOURCE FOR SERPENT

Reaction rate (of DD or DT) in group 2 or 3 is defined by

$$r_{12} = \iiint_{\mathbf{v}_1} \iiint_{\mathbf{v}_2} f_1(\mathbf{v}_1)\, \sigma(|\mathbf{v}_1 - \mathbf{v}_2|)\, f_2(\mathbf{v}_2)\, |\mathbf{v}_1 - \mathbf{v}_2|\, d\mathbf{v}_1 d\mathbf{v}_2, \tag{1}$$

where $f_{\mathrm{j}}(\mathbf{v}_{\mathrm{j}})$ is the velocity distribution function of the particle species j with the velocity $\mathbf{v}_{\mathrm{j}}$, and $\sigma(|\mathbf{v}_{\mathrm{j}} - \mathbf{v}_{\mathrm{k}}|)$ is the velocity-dependent reaction cross section between particles j and k, given by the Bosch-Hale model [7]. In thermal reactions, production rate is simplified to

$$r_{\mathrm{th}} = n_1 n_2 \langle \sigma \mathbf{v} \rangle_{12}(T_{\mathrm{i}}), \tag{2}$$

where n_{j} is the density of the fuel particle species j, and $\langle \sigma \mathbf{v} \rangle_{\mathrm{jk}}(T_{\mathrm{i}})$ is the temperature-dependent reactivity between particles j and k, integrated over the Maxwellian velocity distribution of the thermal particles.

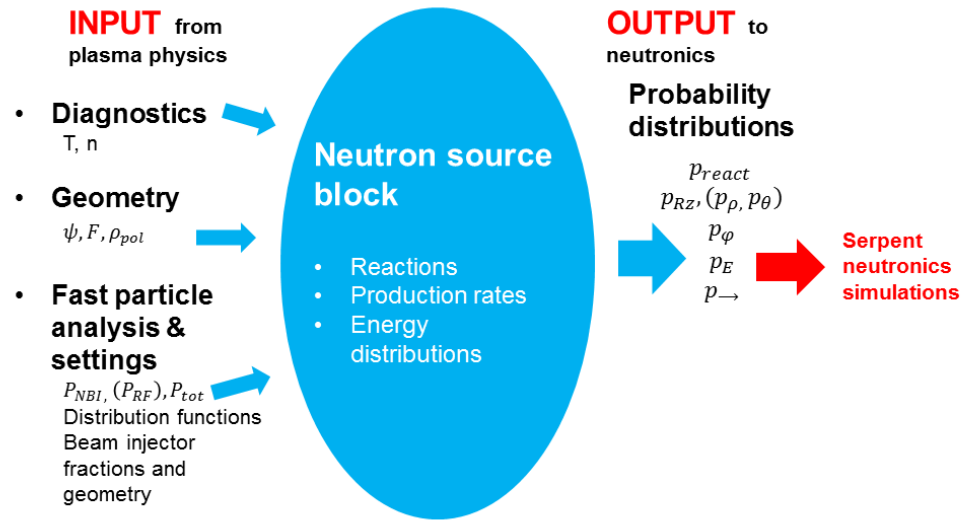

Figure 1. Inputs and outputs of fusion plasma neutron source computing block.

The distribution functions are calculated by ASCOT (Accelerated Simulation of Charged particle Orbits in Tori) which is a fast minority particle orbit following MC code developed in Aalto University and VTT since early 90s [8, 9]. It is a versatile and widely used tool for analyzing different fusion plasmas, especially NBI-heated particle effects in several devices. Generation of a realistic neutron source for Serpent is performed with the AFSI Fusion Source Integrator [10]. AFSI is working as a part of ASCOT, calculating tokamak fusion reactivity and energy distribution of the reaction products, and it is suitable for defining neutron production in all birth channels (groups 1-3).

Plasma-physics-based neutron production model provides the source input to Serpent and computational connection between plasma neutron source and neutronics calculation is illustrated in Figure 1. The source model includes defining of production rates of neutrons in groups (1)-(3) and energy distributions of reaction products in 1.5-2.0-dimensional grid in poloidal plasma cross section. Neutron source can be defined by using (R, z) or (ρ, θ) grid (or alternatively simply 1.5-dimensionally with ρ-coordinate) depending on the input data (required input is presented in the input list in Figure 1) from plasma diagnostics and simulations. The different coordinate systems are presented in Figure 2.

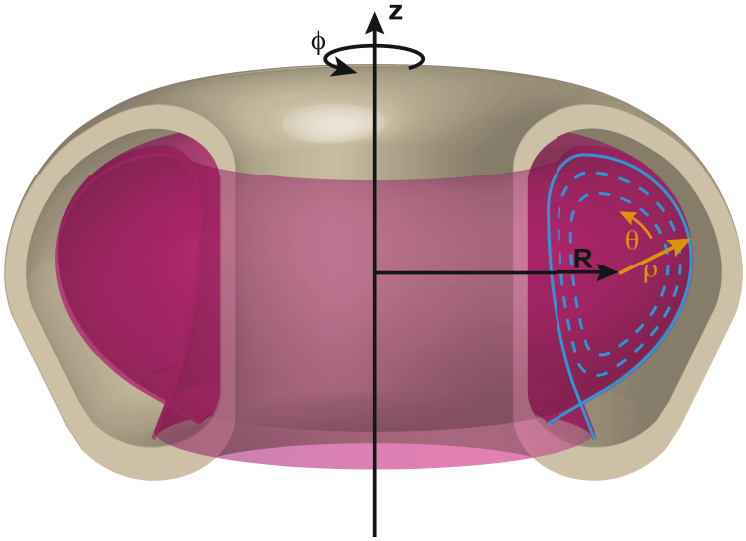

Figure 2. The (R, z) and (ρ, θ) coordinate systems in tokamak geometry.

Benefits of AFSI compared to previously applied methods based on simplified analytical approximations of plasma parameters, such as T and n, include better accuracy of the source geometry (from the magnetic equilibrium solver) and possibility to include all reaction types in the analysis. In addition, AFSI is capable of coupling the neutron source definition to time-dependent plasma transport simulations by, for example, the ETS [11] or JINTRAC [12] packages, which is useful in analysis of yet non-existing devices, such as ITER and DEMO or DT extrapolation of JET, for instance.

Several development steps in the AFSI-based neutron source have been planned. In the current version of the code, all groups of reactions have been taken into account, and flux surface symmetry is assumed. Generating anisotropic energy distribution is under testing. Additionally, neutron source is defined with (R, z) coordinates in AFSI and this will be updated to enable selection between (ρ, θ) and (R, z) coordinates, which makes testing of the efficiency of the method and its sensitivity to small variations in source geometry or plasma parameters more fluent. At the moment, using ρ grid is possible via JINTRAC coupling, which includes the equilibrium solver (transformation from R to ρ).

4. TEST CASE

Baseline and steady-state cases of ITER with $Q = 10$ and $Q = 5$, respectively, and D/T mix of 50%/50% have been used as demonstration cases, and the main parameters are summarized in Table I. The neutron production rates are given in (ρ, θ) coordinates by AFSI coupled to JINTRAC in thermal

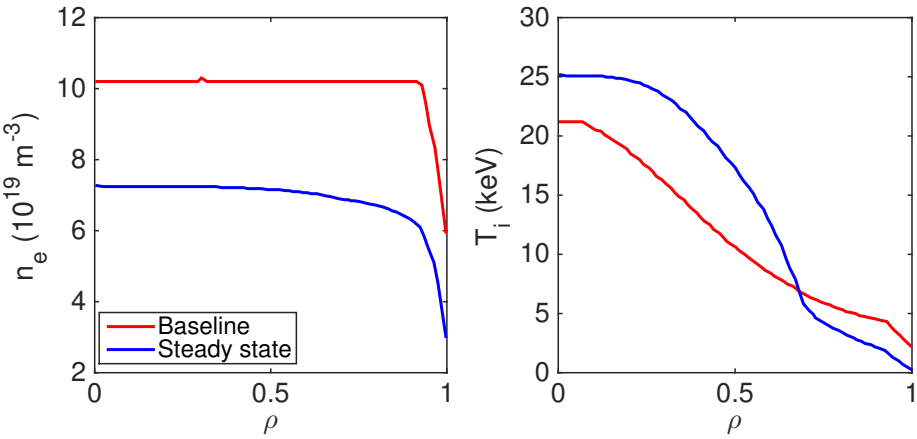

Figure 3. Electron density (left) and ion temperature profiles (right) of the demonstration cases.

and fast-thermal particle reactions. The fast-fast reactions are not considered, since they are not implemented in JINTRAC. However, their contribution in the total neutron production has been shown to be insignificantly small. The electron density and ion temperature profiles of the demonstration cases, given by the ITER database [13], are presented in Figure 3.

Table I. Key parameters of the demonstration cases.

Parameter	**Baseline**	**Steady-state**
Energy multiplication factor Q	10	5
Duration (s)	400	1000
Total source rate (s^{-1})	1.9915×10^{20}	1.8482×10^{20}
Fraction of thermal DD (%)	0.26	0.28
Fraction of thermal DT (%)	99.58	99.52
Fraction of beam-thermal DD (%)	1.011×10^{-2}	1.420×10^{-2}
Fraction of beam-thermal DT (%)	0.15	0.18

The total neutron production rates (thermal) given by AFSI, 2D source geometry and cumulative probability distributions which are used to sample source neutrons are presented in Figure 4. These figures and the neutron sources (see Figure 5) show that the total neutron rate is lower in the steady-state scenario and additionally the rate profile is peaked to the outer radius which causes the maximum source neutron distribution to be further from the magnetic axis than in the baseline case.

The coupling of plasma source to neutron transport simulation is demonstrated by running the baseline and steady-state cases with Serpent 2. Instead of using a conventional CSG-based geometry model,

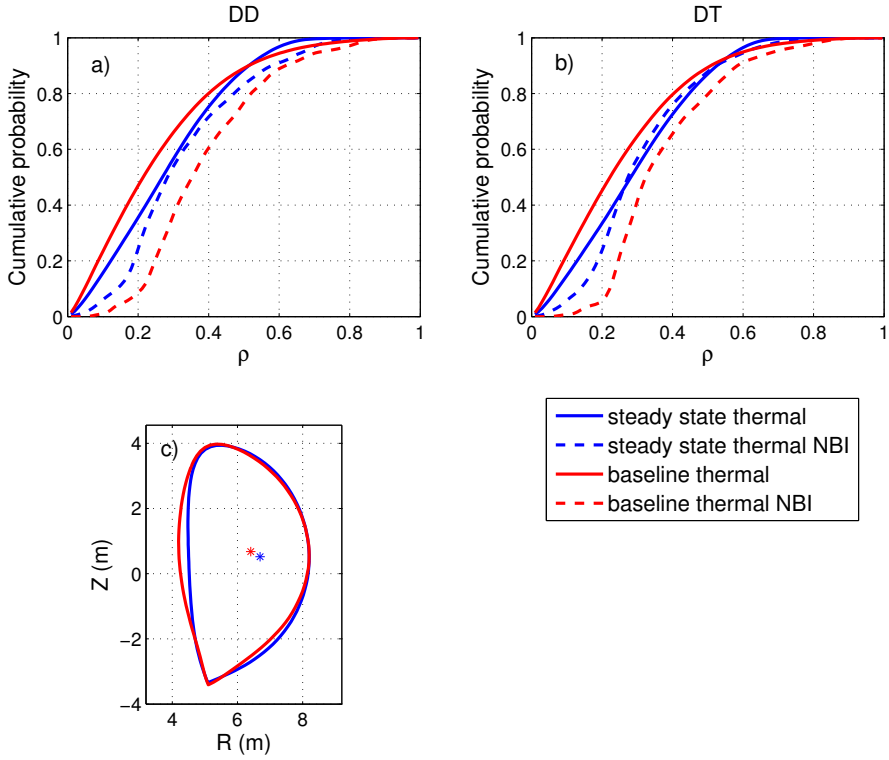

Figure 4. Radial probability of DD (a) and DT (b) reactions based on the radial reaction rates and the plasma shape (c) in demonstration cases.

the C-Lite V1 Rev. 131031 CAD model of the ITER reactor was converted into STL, and imported as-is into Serpent 2. The model and the CAD-based geometry type in Serpent 2 are described in detail in Ref. [1]. Basically the model consists of a total of 11 components, divided into 1,548 solid bodies. There are two major differences in the current geometry model compared to that used in the previous study: 1) a geometry error in one of the STL solids making up the cryostat was fixed, and 2) more realistic material compositions were adopted from an MCNP model of the C-Lite geometry. The geometry is plotted for illustration in Figure 6.

During the course of the study it was discovered, however, that the CSG model prepared for MCNP is not a 100% match compared to the original CAD model. This is especially the case for four parts: blanket, toroidal field coils, vacuum vessel and divertor. Because of this mismatch, certain compromises had to be made when assigning the material compositions to the individual STL solids. The

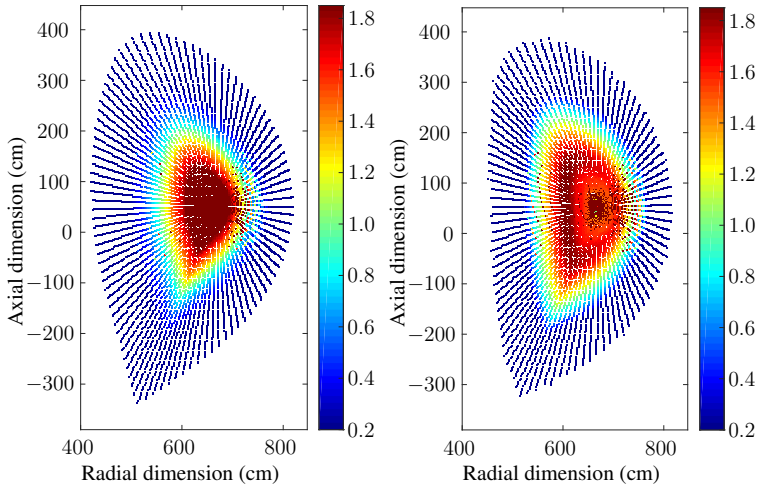

Figure 5. Source distributions of baseline (left) and steady-state (right) cases. The source distributions are discrete in terms of the θ-coordinate.

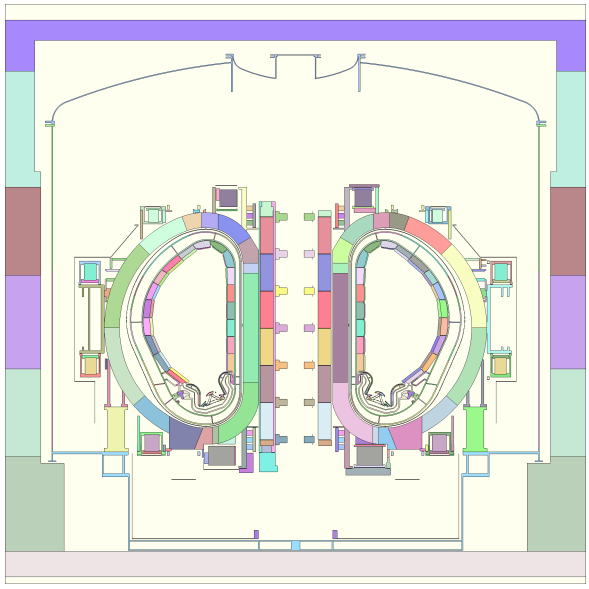

Figure 6. Serpent geometry plot of the CAD-based ITER fusion reactor model (C-LITE V1 Rev. 131031). Different STL solids are plotted with different colors.

impact of these discrepancies in the final results is difficult to assess. More importantly, the CAD-based model used in this study is missing the water-filled regions in various cooling ducts, some of which are located near the first plasma wall. Since these regions act as neutron moderators, neither the spectrum nor the spatial distribution of neutrons obtained from the calculations can be considered realistic representations for an operating reactor.

Despite this unfortunate setback, it was decided to present the results as a demonstration of the available capabilities. The neutronics simulations were performed using FENDL-3.1 based cross section libraries. A total of 200 million neutron histories were run in a 3.47 GHz 12-core Intel Xeon workstation. The overall calculation time was approximately 22 hours for both calculation cases. The flux and absorption rate distributions are calculated using cylindrical mesh tallies with 200 radial and 400 axial bins. The results are presented in Figures 7 and 8.

The same calculations were used to perform material activation for the second part of the study. This was accomplished using the built-in burnup routine in Serpent 2. The results are discussed in a separate paper [2].

5. CONCLUSIONS AND DISCUSSION

In a previous study [1] it was shown that the CAD-based geometry type recently implemented in Serpent 2 is capable of handling complex geometries encountered in fusion applications, such as the C-Lite model of the ITER reactor. The calculations were performed for the purpose of testing the new geometry type, and because of the lack of realistic material compositions and neutron source distribution, the results were not considered physically relevant.

The purpose of this study was to continue the work with a more refined model, including realistic material compositions and neutron source. During the course of the study it turned out, however, that the CAD-model used in the calculations was completely missing the solid components of some water-filled cooling ducts, which are expected to have a major impact on the results of the neutronics simulation. Therefore the results of this study cannot be considered physically realistic either.

Another major goal was to demonstrate in practice the calculation sequence involving the AFSI and JINTRAC plasma scenario codes coupled to Serpent 2 source routine. This goal was accomplished, and the calculation sequence is extended further into material activation and shut-down dose rate calculations in the second part of the study [2].

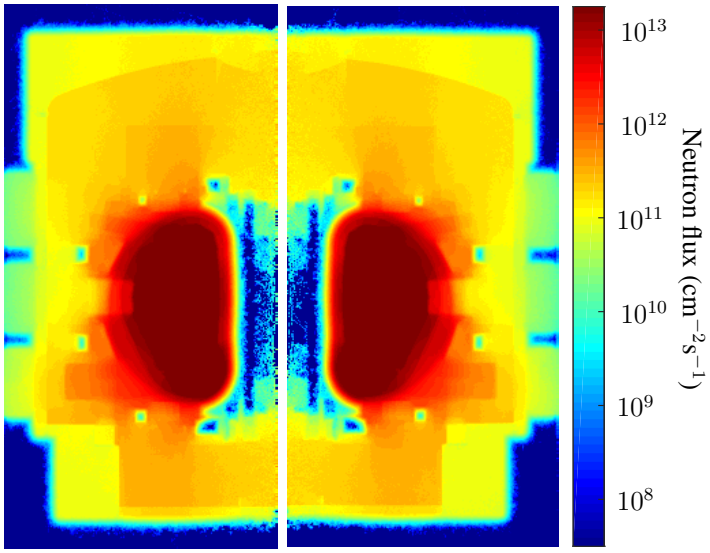

Figure 7. Neutron flux distribution calculated by Serpent. Left: baseline case, Right: steady-state case.

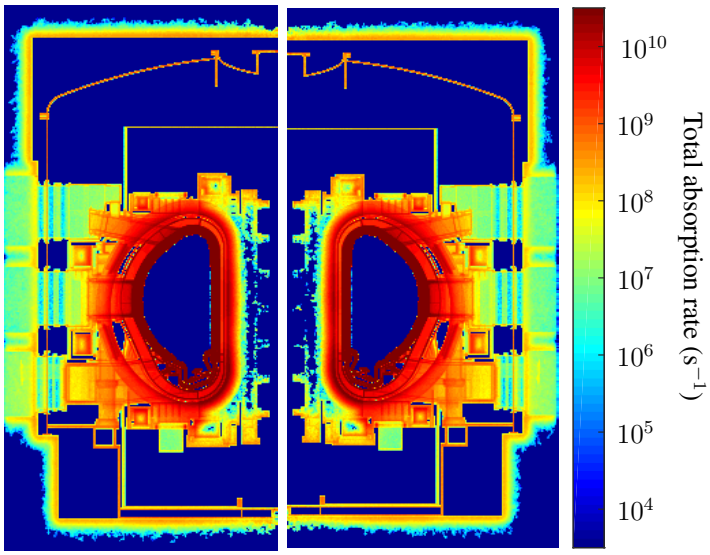

Figure 8. Neutron absorption rate distribution calculated by Serpent. Left: baseline case, Right: steady-state case.

6. ACKNOWLEDGMENTS

This work was carried out using an adaptation of the C-Lite MCNP model which was developed as a collaborative effort between the FDS team of INEST China, University of Wisconsin-Madison, ENEA Frascati, CCFE UK, JAEA Naka, and the ITER organization.

This work has been carried out within the framework of the EUROfusion Consortium and has received funding from the Euratom research and training programme 2014-2018 under grant agreement number 633053 [and from Tekes – the Finnish Funding Agency for Innovation under the FinnFusion Consortium]. The views and opinions expressed herein do not necessarily reflect those of the European Commission.

REFERENCES

[1] J. Leppänen. "CAD-based geometry type in Serpent 2 – application in fusion neutronics." In: *M&C + SNA + MC 2015*. Nashville, TN, USA (2015).

[2] J. Leppänen and T. Kaltiaisenaho. "Expanding the use of Serpent 2 to fusion applications: Shutdown dose rate calculations." In: *PHYSOR 2016*. Sun Valley, Idaho (2016).

[3] J. Leppänen *et al.* "The Serpent monte carlo code: Status, development and applications in 2013." *Ann. Nucl. Energy*, **82**: pp. 142–150 (2015).

[4] J. Leppänen *et al.* "The Numerical Multi-Physics project (NUMPS) at VTT Technical Research Centre of Finland." *Ann. Nucl. Energy*, **84**: pp. 55–62 (2015).

[5] T. Kaltiaisenaho. *Implementing a photon physics model in Serpent 2*. Master's thesis, Aalto University (2016).

[6] J. Leppänen and M. Aufiero. "Development of an unstructured mesh based geometry model in the serpent 2 monte carlo code." In: *PHYSOR 2014*. Kyoto, Japan (2014).

[7] H. Bosch and G. Hale. "Improved formulas for fusion cross-sections and thermal reactivities." *Nucl. Fusion*, **32**: pp. 611–631 (1992).

[8] J. Heikkinen *et al.* "Particle simulation of the neoclassical plasmas." *J. Comp. Phys.*, **173**: pp. 527–548 (2001).

[9] E. Hirvijoki *et al.* "ASCOT: Solving the kinetic equation of minority particle species in tokamak plasmas." *Comp. Phys. Comm.*, **185**: pp. 1310–1321 (2014).

[10] S. Äkäslompolo, O. Asunta, and P. Sirén. "AFSI fusion source integrator for tokamak fusion reactivity calculations." Under preparation.

[11] D. Coster *et al.* "The European transport solver." *IEEE Trans. Plasma Sci.*, **38**: pp. 2085–2092 (2010).

[12] S. Wiesen et al. JET-ITC Report (2008).

[13] "ITER Database." In: *user.iter.org*.

Aalto-DD 118/2018
VTT SCIENCE 180

ISBN 978-952-60-8046-8 (printed)
ISBN 978-952-60-8047-5 (pdf)
ISSN 1799-4934 (printed)
ISSN 1799-4942 (pdf)

978-951-38-8651-6 (printed)
978-951-38-8650-9 (pdf)
2242-119X (printed)
2242-1203 (pdf)

Aalto University
School of Science
Department of Applied Physics
www.aalto.fi

BUSINESS + ECONOMY

ART + DESIGN + ARCHITECTURE

SCIENCE + TECHNOLOGY

CROSSOVER

DOCTORAL DISSERTATIONS